Team 83 Project Technical Report to the 2026 IREC

Rowan University Rocketry Team *

Rowan University, Department of Mechanical Engineering and Department of Computer and Electrical Engineering, Glassboro, New Jersey

The Rowan Rocketry team is submitting this Project Technical Report in support of its entry to the Intercollegiate Rocket Engineering Competition (IREC), hosted by the Experimental Sounding Rocket Association (ESRA). The team is competing in the 10,000 ft Commercial Off-The-Shelf (COTS) solid motor category, utilizing a high-power launch vehicle designed with an emphasis on reliability, safety, and disciplined systems integration. The vehicle incorporates a modular architecture consisting of five primary subsystems—Airframe (Structures), Propulsion, Recovery, Avionics, and Payload—each developed to satisfy performance, manufacturability, and competition constraints. The rocket is designed to carry a competition-compliant payload while achieving a target apogee of 10,000 feet and ensuring safe, repeatable recovery through a dual-deployment parachute system. The Payload subsystem is designed to maintain a stable internal ambient temperature and pressure environment using layered insulation while serving as the required competition payload carried by the launch vehicle. The mission objective is to demonstrate a fully integrated and validated rocket system capable of meeting competition requirements while reflecting a rigorous, analysis-driven engineering approach. Required testing included subsystem verification, avionics functionality checks, recovery deployment testing, structural and fit inspections, propulsion integration checks, and full-system integration reviews. Testing was used to confirm that the launch vehicle could safely integrate its major subsystems, meet competition requirements, and support a controlled launch and recovery sequence.

I. Nomenclature

COTS = Commercial-Off-The-Shelf

SRAD = Student Researched and Developed

FMECA = Failure Modes, Effects, and Criticality Analysis

FOS = Factor of Safety

FEA = Finite Element Analysis

CFD = Computational Fluid Dynamics

QFD = Quality, Function, Deployment

**James Lee, Sarah Ely, Nolan Heaney, Jakub Gajda, Shawn Smith, Jeremiah Francois, Harrison Roy, Marian Yanka, Marcelo Bisicchia, Thomas Rasa, Anchal Patel, Keven Guzman, Noelle Ross, Brody Schneider, Paul Porreca, Vanessa Hutchinson, Kuba Jagoda, Dean Siedlecki, Jared Crane, Chris Rios, Joe Mihalik, Max Bykov, Dharma Upadhyay, Emma Ferrarese, Bruce Durham, John Radulic, Aiden Aschoff, Victoria Van, Justin Dougherty*

II. Introduction

A. Competition Category and Vehicle Overview

Rowan Rocketry is competing in the 10,000 ft Commercial Off-The-Shelf (COTS) category of the Intercollegiate Rocket Engineering Competition (IREC), hosted by the Experimental Sounding Rocket Association (ESRA). Teams in this category design, build, test, and launch high-power rockets carrying a minimum 4 lb payload to a target apogee of 10,000 ft. The Rowan Rocketry launch vehicle incorporates a reliability-focused design emphasizing manufacturability, structural robustness, and repeatable performance. The system is divided into five subsystems: Airframe, Propulsion, Recovery, Avionics, and Payload, developed under constraints related to competition rules, structural limits, cost, and schedule.

B. Payload Mission

The Payload subsystem participated in the SDL Payload Challenge, developing a passive payload designed to maintain ambient temperature and pressure inside the payload bay. The system uses internal insulation and onboard sensors to monitor environmental conditions, simulating the protection of a miniature human passenger.

C. Project Goals and Objectives

This vehicle is Rowan Rocketry's third IREC rocket since returning to competition in 2024. Lessons learned from prior flights: particularly schedule compression, limited testing, and recovery-system complexity, motivated a design approach centered on simplicity, reliability, and increased testing. The primary goals for this year include achieving a nominal 10,000 ft flight, improving subsystem integration, validating avionics and recovery performance, and strengthening documentation and traceability.

D. Academic Program

Rowan Rocketry operates within Rowan University's Engineering Clinic Program, a required, hands-on design sequence for all engineering majors. The clinic provides multidisciplinary project experience emphasizing system integration, technical communication, and iterative design. Students from mechanical, electrical, and computer engineering collaborate on long-term efforts such as IREC, with many members participating for multiple semesters to support continuity and knowledge transfer.

E. Team Structure

The team is organized into five subsystems: Airframe, Propulsion, Recovery, Avionics, and Payload. Each is led by a subsystem lead responsible for design decisions, documentation, and coordination. All leads report to the Team Captain, who manages system-level integration and project direction. Most members are mechanical engineering students, with electrical and computer engineering responsibilities concentrated in the Avionics subsystem. A Logistics Coordinator supports documentation, scheduling, and communication with faculty.

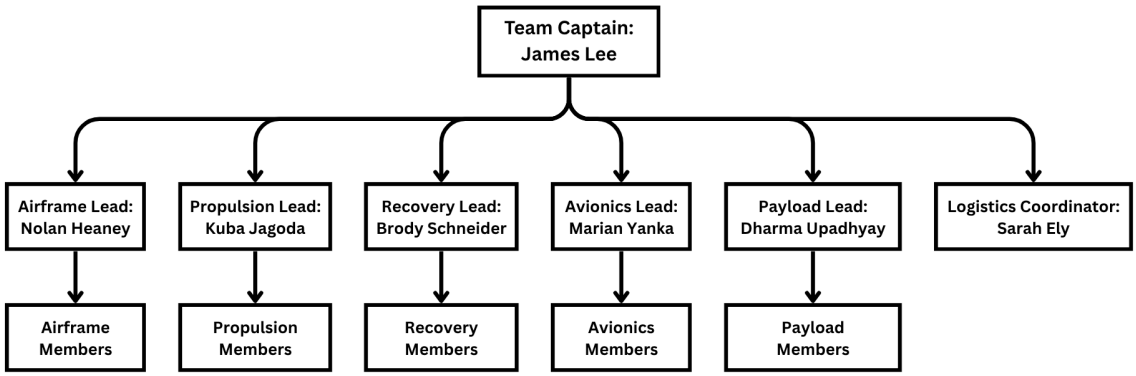


Fig. 1: Team Organizational Structure

F. Management Strategy

Project execution relied on structured collaboration and documentation across subsystems. A shared Google Drive served as the central repository for reports, presentations, and planning materials, while GitHub provided version control for CAD models, PCB designs, and simulation files. Major design decisions were supported by Quality Function Deployment (QFD) matrices (shown in Appendix G) and Failure Modes, Effects, and Criticality Analysis (FMECA) (shown in Appendix D) to evaluate performance, manufacturability, cost, and risk. A detailed Gantt chart tracked milestones, subsystem deliverables, and integration timelines to maintain schedule alignment.

G. Stakeholders

The project is supported by faculty advisors, university machine shops and fabrication facilities, and commercial vendors supplying materials, propulsion components, and avionics hardware. Funding is provided through Rowan University, departmental support, and external sponsors.

H. Report Preparation

The Project Technical Report was prepared collaboratively. Subsystem leads drafted their respective sections, while the Team Captain and designated editors integrated content, ensured consistency, and aligned the document with IREC formatting requirements. All figures, analyses, and subsystem descriptions underwent team review to maintain technical accuracy.

III. System Architecture Overview

A. Overview of the System

The rocket is composed of six main subsystems: aero-structures, propulsion, avionics, recovery, telemetry, and payload. The aero-structure comprises the entire outer structure of the rocket, including the nose cone, body tube, fins, and boat tail, which is responsible for withstanding the loads during the rocket's flight. The propulsion subsystem consists of a motor which contains enough power for the rocket to reach its desired altitude of 10,000 feet and a motor mount to transfer loads from the motor to the

vehicle structure. The avionics subsystem is integrated within the avionics bay, which is housed within a bulkhead in a central coupler shown in Figure 2, which contains two flight computers, an altimeter, and a GPS. The recovery subsystem contains a main parachute and drogue parachute housed inside separate bulkheads with black powder inside charge wells. The telemetry subsystem is responsible for offboard communication to the ground station computer. The payload subsystem is a box with electrical components with a 2 kg weight requirement that contains 3D printed figurines to monitor temperature changes throughout the flight of the rocket.



Figure 2: Visual overview of fully integrated launch vehicle and major subsystems

B. Airframe Subsystems

1. Overview

The airframe and fins subsystem provides the primary structural and aerodynamic foundation of the launch vehicle, maintaining integrity under axial, bending, and torsional loads during ascent and recovery while ensuring stability and interfacing with propulsion, avionics, recovery, and payload systems. Design decisions within this subsystem directly influence mass distribution, stability margin, and overall flight reliability. The airframe utilizes commercially available (COTS) fiberglass body tubes sourced from Wildman Rocketry to reduce manufacturing risk and ensure dimensional consistency. This approach introduces constraints in geometry, material properties, and coupling interfaces that drive internal layout and structural integration decisions. Structurally, the airframe must withstand motor thrust, aerodynamic forces, and recovery loads while maintaining alignment of internal components and protecting onboard electronics. Aerodynamically, the fin configuration and external geometry provide sufficient static stability without excessive drag or aeroelastic risks such as fin flutter, constraining fin geometry and material selection.

2. Internal Layout

The internal layout was established early in the design process because the placement of the payload, recovery system, avionics bay, structural bulkheads, and propulsion system directly affects vehicle length, mass distribution, stability, and integration accessibility. OpenRocket and the full CAD assembly were used to estimate the size, position, and mass of each internal component, ensuring sufficient packaging volume while maintaining a favorable center of gravity and stability margin for flight.

From front to rear, the vehicle consists of the nose cone, a 20-inch payload tube, the recovery bay, avionics bay, sustainer tube, and motor mount assembly. The nose cone and payload tube are permanently bonded with a fiberglass coupler to form a rigid forward body, while a machined payload

holder secures the payload mass. A CNC-machined bulkhead separates the payload from the recovery bay and provides an interface for recovery hardware. The drogue parachute is housed directly behind this bulkhead for forward deployment. Behind the forward body, the avionics bay is built around a 16-inch fiberglass coupler with a 4-inch switch band for external arming access and is enclosed by two CNC-machined aluminum bulkheads that protect electronics from ejection gases while serving as structural attachment points. The aft section contains the main parachute and propulsion system, separated by an internal bulkhead, with the motor mount and fin assembly located at the rear. This configuration preserves a conventional and reliable layout while supporting modular avionics integration, recovery accessibility, and favorable stability characteristics.

3. Body Tube Material

Material selection for the body tube was guided by a Quality Function Deployment (QFD) decision matrix comparing Blue Tube with fiberglass wrap, fiberglass, and carbon fiber (Appendix G-A). A key constraint was the requirement for pre-manufactured, pre-cut tubing to reduce machining time and allow greater focus on integration. Based on this analysis, fiberglass body tubes were selected due to their balance of strength, availability, and compatibility with existing components. The airframe maintains a 6-inch diameter, with an 8-inch coupler used to permanently bond the nose cone and payload section, and a 16-inch coupler used for modular connections between major subsystems.

4. Nose Cone Shape

The nose cone is a key aerodynamic and structural component, reducing drag while influencing stability, mass distribution, and packaging. Because the vehicle operates near the transonic regime, selection was based on aerodynamic performance, mass, material compatibility, and availability. Several profiles were evaluated, including Von Karman, tangent ogive, parabolic, and power-series geometries. As shown in Appendix G-F, drag coefficient differences between rounded profiles are minimal near the expected flight speed of approximately Mach 0.9. Cone and ellipsoid shapes were excluded due to higher drag, leaving the 5:1 Von Karman and 4:1 tangent ogive fiberglass nose cones as the primary candidates. A Quality Function Deployment (QFD) decision matrix was used to compare these options, weighting drag (35%), material compatibility (30%), weight (25%), and cost/availability (10%).

The tangent ogive achieved the highest score (6.9) compared to the Von Karman (5.4), indicating a better overall balance of performance, manufacturability, and availability (Appendix G-E). Although the Von Karman profile has been used successfully on previous vehicles, the tangent ogive offered practical advantages. Its shorter 4:1 length-to-diameter ratio reduced overall length and mass while maintaining comparable performance. Simulations predicted apogees of 12,352 ft for the tangent ogive and 12,217 ft for the Von Karman, a difference of approximately 1.1%, which is negligible relative to real-world uncertainties. Based on these results, the team selected the 4:1 tangent ogive fiberglass nose cone for its balanced performance, reduced length, and compatibility with design constraints.

5. Structural & Laminating Epoxy

Structural epoxy is used to bond the fins to the motor tube and reinforce the external airframe. Epoxy selection was performed using a QFD weighted decision matrix (Appendix, Table X), comparing candidates based on mechanical properties, viscosity, cost, and workability. U.S. Composites 635 was

selected for its strong tensile and compressive performance, low cost, and manageable pot life. Due to its low viscosity, it is thickened with colloidal silica for structural bonding applications to improve handling and gap-filling capability. For carbon fiber layups, the same epoxy system is used without additives, allowing it to function effectively as a laminating resin. This approach simplifies material usage by consolidating both structural bonding and layup processes into a single epoxy system while maintaining adequate performance.

6. Boat Tail

The boat tail is a newly introduced aerodynamic component used to reduce base drag and improve overall efficiency during ascent. By tapering the aft diameter of the rocket, it reduces flow separation at the base. A parabolic profile for the boattail was chosen for enhanced performance at lower mach number to transonic flight conditions [10]. The primary structure consists of a carbon fiber shell, selected for its high strength-to-weight ratio and smooth surface finish. The mounting interface is a custom two-part locking mechanism manufactured using a carbon fiber–reinforced high-temperature thermoplastic (Fibreheart™ PPA-CF). This material was chosen for its mechanical strength and thermal resistance, which are critical due to the proximity to the motor during operation. The lower portion of the mechanism is attached to the aft centering ring using threaded fasteners, while the upper portion is bonded to the carbon fiber shell. The assembly is installed by sliding and rotating the components into a locked position via a set screw, ensuring alignment and load transfer.

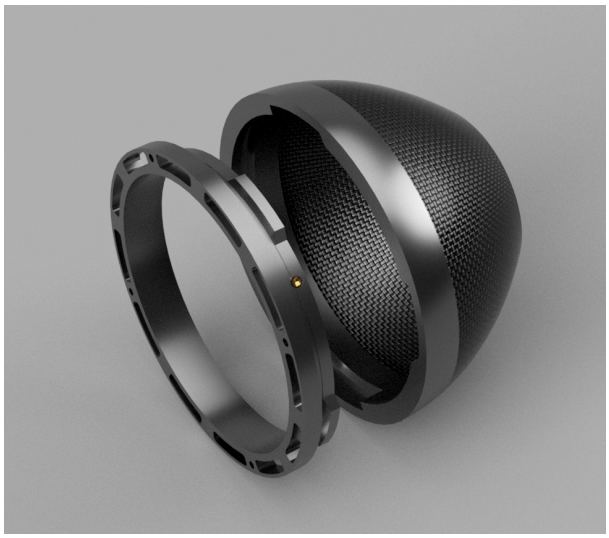


Figure 3. Boat Tail Exploded View

7. CFD Analysis of the Boat Tail

Because our primary simulation software (Open Rocket), does not have the capability to simulate a parabolic profile, a CFD study was run in ANSYS Fluent to analyze drag on this design. For this study, two transient simulations modeling Night Owl with and without the boat tail were run. These simulations were run at the flight regimes peak velocity of 333 [m/s] or Ma = 0.964 at an altitude of 800 [m] (See Appendix A-D). For lack of atmospheric data 800 [m], Temperature, pressure and density for atmospheric conditions at 1 [km] were approximated and input as boundary conditions for the model [9]. To accurately model drag at our peak velocity, some assumptions were made. These assumptions include:

Transonic Flight Regime Assumptions: Night Owl reaches a peak Mach Number of 0.964 at motor burnout. For this reason, the energy equation, compressibility, and viscous heating effects are turned on in the model according to the Ideal Gas Law for variable ρ, and Sutherland's Law for variable μ.

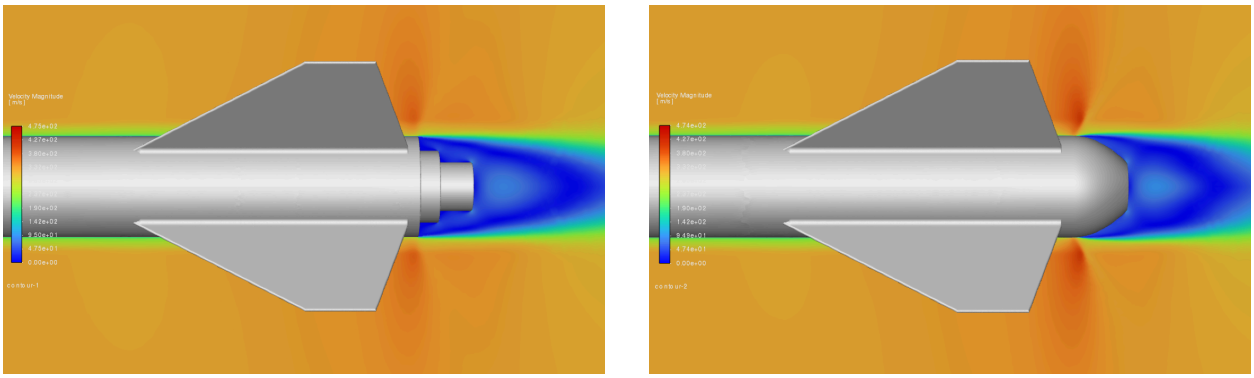
Reynolds-Averaged Navier–Stokes (RANS) Based Model Assumptions: K-ω SST turbulence model was used, as K-ω SST blends K-ω at near wall regions and k-ε at far field, for more accurate wall shear force without using enhanced wall treatment.

Using a calculated Reynolds Number of Re = 5.755 x 10^7 for the body tube, boundary layer calculations were performed. Initial mesh inflation layer height for the body tube was found to be 6.1 x 10^-5 [m] using a yplus calculator from CFDonline. With a target yplus of 40, growth ratio of 1.3, and initial inflation layer height seen above, the number of inflation layers needed to encapsulate the boundary layer height were calculated as seen in Figure 4 below. All additional calculations for fins and aft sections can be found in Appendix G-AC.

$$\delta_{99} = \frac{0.38L}{\sqrt[5]{Re}} = \frac{0.38 \times 2.8}{\sqrt[5]{5.755\times10^{7}}} \equiv y_{Inflation} = \frac{(1-G^{N})}{(1-G)} y_0 = \frac{(1-1.3^{N})(6.1\times10^{-5})}{(1-1.3)} \rightarrow N = 11 \text{ Layers}$$

Figure 4. Body Tube CFD inflation Layer Calculations

Once mesh settings were finalized, two transient simulations were run for 500 iterations at 0.1 [ms] intervals for a total flow time of 0.05 [sec]. The two CFD simulations predicted *no change in drag* at a flow speed of Ma = 0.964. While this is opposite of what was initially predicted by openrocket simulations, the flow separation is still quite large behind the boat tail as seen in Figure 5a, and 5b. These results were interpreted to find that future iterations of the boattail should be extended from 0.1 to 0.25 [m] in length to prevent flow separation at higher mach numbers. More work on CFD needs to be done, as it is likely there is less flow separation at lower velocities, however at our peak velocity, drag is not affected. Numerical values for drag can be seen in Appendix G-AD, G-AE.

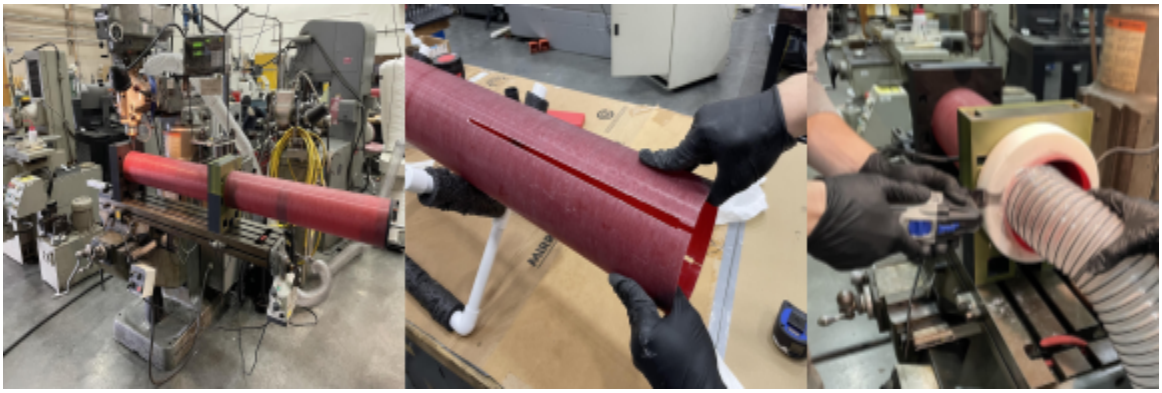


Figures 5A, 5B. CFD velocity cut plots at 50 [ms], (Left) No Boat Tail, (Right) Parabolic Boat Tail

8. Body Tube Machining

Machining of the fiberglass body tubes was required to produce accurate fin slots, structural interfaces, and final airframe lengths. In previous years, the team used a custom fixture consisting of 8020 extrusions, threaded rod, and 3D-printed end caps with an indexing system that allowed the tube to be rotated and locked at precise angular increments for repeatable operations such as 90-degree fin placement.

The transition to fiberglass airframes introduced new constraints, as machining was not permitted at Rowan University due to airborne particulate concerns. External machining options were explored but were not feasible due to cost and availability. This limitation was overcome through collaboration with the Camden County College CIM Center, which provided appropriate facilities and improvements to the fixture design. Additional 3D-printed supports were incorporated to reduce vibration and improve stability during machining, as shown in Figure 6A. Using this setup, fin slots were machined at precise 90-degree intervals along the sustainer tube, maintaining alignment with the motor mount and fin assembly. A longitudinal slit was also cut from each slot to the aft end of the tube to allow slight expansion during insertion of the integrated motor mount assembly (Figure 6B). Body tube length cuts were performed using the same fixture, with a 3D-printed sleeve acting as a reference face to ensure clean, perpendicular cuts (Figure 6C). Throughout all operations, appropriate PPE and dust mitigation strategies, including local vacuum extraction and forced airflow, were used to minimize exposure to fiberglass particulates.



Figures 6 A - C. (Left) Body Tube Mill Fixture Setup, (Middle) Machined Fin Slots, (Right) Body Tube Length Cutting Setup

9. Body Tube Testing

Due to the absence of several critical G12 fiberglass material properties required for buckling analysis, material testing was performed to determine representative mechanical properties for the body tube. Compression testing was conducted on two samples, and the resulting data was extrapolated to estimate additional material properties needed for the tension and shear stress analyses. The G12 fiberglass was tested in compression using ASTM D695, while tensile and shear properties were evaluated using ASTM D3039 and ASTM D5379, respectively. The average values obtained from each test standard are listed in Appendix G-G.

A buckling test was simulated in ANSYS to confirm the structural integrity of the sustainer. A linear buckling analysis followed by a nonlinear counterpart was created. Due to the scarce amount of reliable resources on G12 fiberglass, the initial material applied to the simulation was Epoxy E-Glass UD in the ANSYS material library. Since G12 fiberglass is a specialized type of E-grade fiberglass, this was our best initial step. Following the receipt of material data detailed in Appendix G-G**,** the analysis was redone and showcased simulated buckling load

of approximately 20 MPa in pure compression. This correlated to approximately 21000 N of force to cause buckling yielding a factor of safety of 9.13. This validates our structural integrity of the sustainer and use of G12 fiberglass. As shown in Figure 7 below, the maximum deformation of the body tube at 20 MPa is 0.00236 m, which is well within the elastic limit of the material.

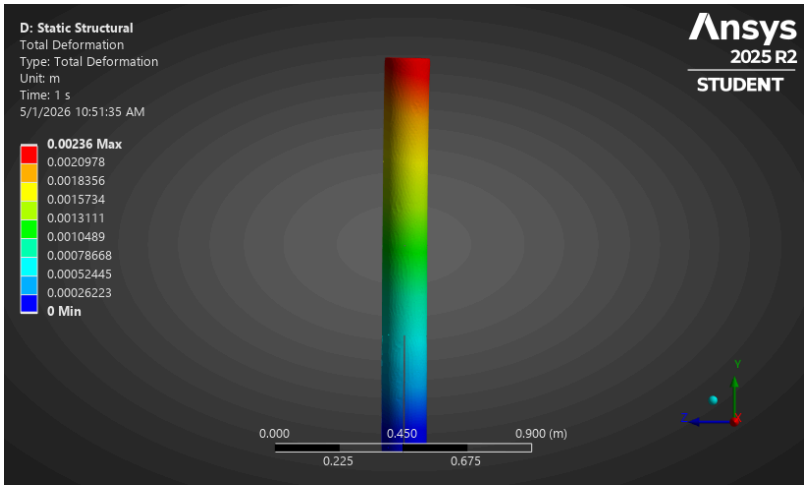


Fig 7. Deformation distribution plot from buckling simulation in ANSYS with values labeled

10. Paint and Thermal Testing

The choice of paint job this year resulted in additional analysis performed to validate the feasibility of dark themed rocket in the hot Texas environment. Initially, it was a decision between paint and vinyl wrap, but paint was ultimately selected due to vinyl's difficult workability [1] and darker colors are prone to warping in extreme temperatures [2]. Furthermore, spray paint is generally recommended for rockets [3] due to its durability that counters a high upfront cost of application [4], but darker colors could accelerate the degradation of the paint [5]. Finally, the rocketry team had more experience with applying paint as opposed to vinyl wrap. After evaluating the benefits and drawbacks of each option, it was decided that paint would be an optimal choice over vinyl wrap, and the next decision was the color of the paint for the rocket that didn't significantly compromise rocket performance.

In order to determine if the color of the paint would significantly impact the rocket's performance it was paramount to ensure that the rocket's internal temperature did not exceed limits. The area that would be most affected by high rocket temperature would be the electronics in the avionics bay, namely the batteries as they have the lowest ceiling for operational temperature at around 60°C. In order to determine the internal temperature of the rocket, a model in Matlab Simulink was created. This model mainly focused on the solar radiation from the sun and the resulting heat transfer to the internals of the

rocket. For this model, a coat of black paint was used as it is the color with the highest absorptivity [6], and if there are no issues with it, then no other color will affect the performance of the rocket. A thermal camera was used (Appendix G-H) in order to verify the veracity of the Simulink model. A comparison of the external temperature of the fiberglass computed by the model (Appendix G-I) and by the thermal camera yielded similar results. Therefore the temperature predicted by the model for the internal battery temperature should be reasonably accurate. As seen in Appendix G-I this value is approximately 47°C which is well below the limit of 60°C. This indicates that even a coat of black paint will not negatively affect the rocket's performance, which allows the use of any color for the rocket's paint job.

C. Fins

1. Center of Pressure & Stability Factor

The fins provide aerodynamic restoring forces that stabilize the rocket during flight by maintaining the center of pressure aft of the center of gravity. The separation between these two points, expressed as a stability margin in calibers, is a primary measure of flight stability.

For this vehicle, a target stability margin of approximately 1.0–1.8 calibers was selected to balance stability and aerodynamic efficiency. While increased stability improves flight robustness, excessive margin can introduce additional drag and reduce overall performance. Stability was evaluated using OpenRocket simulations and incorporated directly into fin sizing and placement decisions.

2. Fin Shape

Fin shape selection was performed to balance aerodynamic efficiency, structural strength, and manufacturability. Several common fin geometries were evaluated, including delta, rectangular, swept, trapezoidal, and tapered configurations. A qualitative comparison of these options, along with a QFD decision matrix, was used to assess performance based on flutter resistance, weight, aerodynamic efficiency, and stability (Appendix G-J, G-K, G-L).

From this analysis, the trapezoidal fin shape was selected as the optimal configuration. This geometry provides a favorable balance between aerodynamic performance and structural robustness while maintaining manufacturability and reliable center of pressure behavior. Additionally, trapezoidal fins offer sufficient flutter resistance within the expected flight regime without introducing unnecessary complexity or fabrication challenges.

The final fin geometry was then sized to meet stability requirements, targeting a stability margin within the desired range while ensuring adequate structural performance during ascent and recovery. Detailed fin dimensions and drawings are provided in Appendix F-E.

3. Fin Material & Strength Analysis

Fin material selection was driven by structural performance, flutter resistance, and availability. Candidate materials were evaluated using a QFD decision matrix considering strength, cost, and manufacturability (Appendix G-D). Based on this analysis, G10 fiberglass (non-FR4) was selected due to its availability and adequate mechanical performance, despite having slightly lower strength and impact resistance compared to alternatives such as G11.

Flutter performance was evaluated using MATLAB-based analysis adapted from prior team work. Initial results indicated that G10 alone did not provide sufficient stiffness to achieve the desired factor of safety. As a result, carbon fiber tip-to-tip layups were incorporated to increase bending stiffness and improve flutter resistance.

Due to limited manufacturer data, representative shear modulus values for G10 and carbon fiber were used in the initial analysis. Additional material testing is planned to refine these inputs and improve model accuracy. Current simulations indicate that 3–4 layers of carbon fiber are required to achieve a fin flutter factor of safety greater than 1.5. Detailed analysis results are provided in Appendix G-M.

4. *Shear Testing*

Due to limited material data for the G10 fiberglass and carbon fiber reinforcement used on the fins, in-house shear testing was performed to validate material strength and obtain properties for analytical and simulation work. Testing focused on determining the shear modulus of G10 fiberglass and carbon fiber bonded with US Composites 635 epoxy, since this value was required to estimate fin flutter velocity and calculate the factor of safety.

Specimens were prepared in accordance with ASTM D3518M by cutting flat material coupons at 45° relative to the fiber direction. Each specimen was loaded in tension until failure while a high-speed camera recorded the test. Six total tests were performed, including three G10 specimens and three carbon fiber specimens. The resulting data were used to generate stress-strain curves and estimate material properties. Through testing, the shear modulus was found to be $G = 2.6 \times 10^6$ psi for G10 fiberglass and $G = 7.6 \times 10^6$ psi for carbon fiber. The test setup is shown in Figure 8A, and a fractured G10 specimen is shown in Figure 8B.

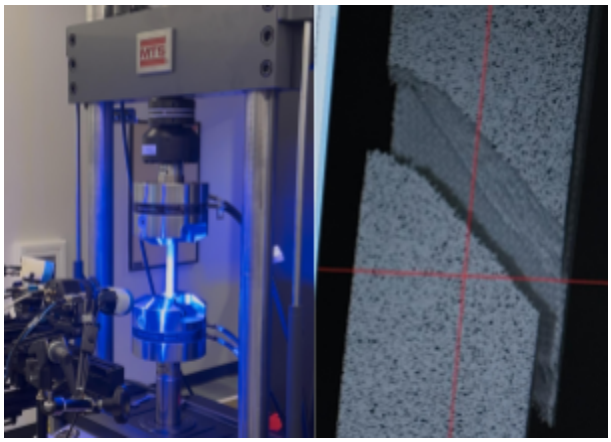


Fig 8 A-B: (Left) Shear Testing Setup, (Right) Close-up View of a Fracture Resulting from Shear Testing on G10

5. *Carbon Fiber Layup*

To improve structural integrity and flutter resistance, three tapered carbon fiber layers were applied tip-to-tip over the G10 fin core. This created a continuous load path across the airframe and

increased bending stiffness under aerodynamic loading. The number of layers was selected from flutter analysis, which indicated that additional stiffness was required to achieve an acceptable factor of safety.

Each layer used a tapered geometry, with the largest layer spanning the full fin and smaller layers placed progressively toward the center. This reduced stress concentrations and encouraged more uniform load distribution. The layups were performed using unthickened US Composites 635 epoxy, selected for its low viscosity and ability to fully wet out the carbon fiber. Bonding surfaces were sanded before layup, and peel ply was applied to remove excess resin and produce a uniform finish. Vacuum bagging was not used; however, care was taken to ensure proper fiber wet-out and consolidation. The resulting composite structure increased stiffness with minimal added mass, improving resistance to flutter and aerodynamic deformation.

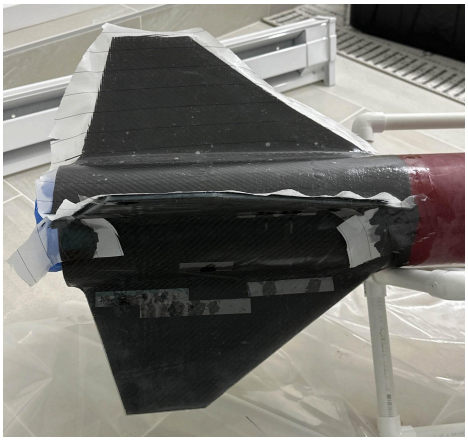


Fig 9: Carbon Fiber Layups with Peel Ply

D. Propulsion Subsystems

1. Overview

The propulsion subsystem is responsible for selecting and integrating a rocket motor capable of achieving the target apogee of 10,000 [feet] while maintaining safe and stable flight characteristics. The system utilizes commercially available (COTS) solid rocket motors, making performance prediction and margin assessment central to the design. Propulsion decisions directly influence structural loading, aerodynamic stability, recovery sizing, and avionics timing.

Motor selection was guided by analytical and simulation-based tools, including OpenRocket and RASAero II. Five candidate motors were evaluated based on apogee, thrust-to-weight ratio, rail departure velocity, and expected Mach number. Because COTS motors have fixed thrust curves and mass properties, analysis focuses on how motor performance interacts with vehicle mass, drag, and stability rather than optimizing the motor itself.

In addition to meeting altitude requirements, the propulsion system must ensure safe rail departure and avoid excessive dynamic pressure or structural loading. Metrics such as thrust-to-weight ratio, off-rail velocity, and peak acceleration were treated as safety-critical design constraints. The subsystem also includes the mechanical integration of the motor through the motor mount assembly,

which transfers thrust loads to the airframe and accommodates ignition and recovery interfaces. Design decisions were guided by a reliability-first approach, prioritizing proven hardware, conservative margins, and repeatable integration methods.

2. Motor Selection

Motor selection was conducted using OpenRocket and RASAero II to evaluate multiple M-class solid rocket motors (Appendix G-N). Rather than targeting an exact apogee, the team selected a motor with a modest performance margin above the 10,000 ft requirement to account for real-world uncertainties such as aerodynamic losses, manufacturing tolerances, and environmental conditions. Several candidate motors satisfied baseline performance requirements; however, cost, availability, and existing hardware influenced the final decision. The AeroTech M2000R was selected due to its ability to meet altitude and thrust requirements while minimizing cost. This motor was also previously purchased and remained unused in controlled storage, eliminating an estimated $1,000 procurement cost.

Simulation results (Appendix A-D) indicate that, at an estimated vehicle mass of 60.6 lb, the selected motor achieves a rail departure velocity of 26.3 m/s and an apogee of approximately 11,079 ft. This provides a margin of roughly 10% above the target altitude, which is appropriate given the absence of active trajectory control systems such as airbrakes and reduces the risk of underperformance. The M2000R also provides acceptable acceleration and velocity profiles, maintaining safe flight conditions without excessive structural loading. Overall, the selection reflects a balance between performance, reliability, and resource efficiency. A graph of the M2000R thrust curve can be found in Appendix G-O.

3. Motor Mount Assembly

The motor mount assembly serves as the primary structural interface between the propulsion system and airframe, transferring thrust loads from the motor into the vehicle structure. It consists of two 6061 aluminum centering rings connected by a section of 4-inch Blue Tube, which maintains alignment of the motor within the airframe (Figure 10).

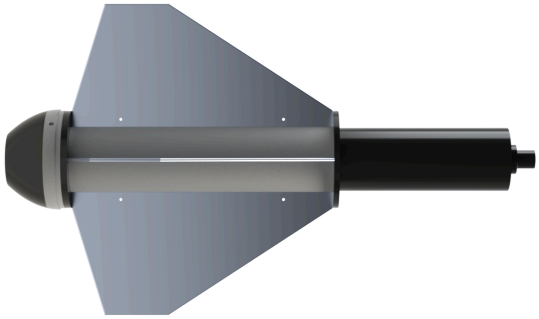


Fig 10: CAD Model of Motor Mount Assembly

Construction of the motor mount began with the fabrication of the centering rings using 6061 aluminum stock. These components were student-machined on lathe and milling machines at Rowan University to achieve the required tolerances and geometry. The use of aluminum provides sufficient

strength to transfer thrust loads while maintaining a manageable weight. Detailed technical drawings of the centering rings are included in the Appendix. Figure 11A shows the machining process for these components.

The motor tube itself was constructed from commercially available 4-inch Blue Tube, which was cut to length based on the vehicle's internal layout. Blue Tube was selected for this application due to its low weight, cost-effectiveness, and adequate structural performance for its role as an alignment tube. Because the motor tube primarily functions to maintain concentric alignment of the motor rather than carry significant structural loads, the use of fiberglass was not necessary, allowing for mass savings and reduced cost without compromising performance.



Fig 11 A-C: Centering Ring Machining (Left), Finished Motor Mount Assembly (Right), Motor Mount Insertion into Sustainer Tube (Right)

Following fabrication of the individual components, the fins were attached to the motor tube using a through-the-wall configuration. To ensure proper alignment, custom 3D-printed jigs were used to position the fins at precise 90-degree intervals around the motor tube. These jigs interfaced with holes designed into the fin tabs, allowing for accurate placement during the initial bonding process. Structural epoxy was used to tack the fins in place, after which thick fillets were applied along the fin roots using additional epoxy. Painter's tape and shaping tools, such as wooden sticks, were used to form consistent fillets, increasing the bonded surface area and significantly improving load transfer between the fins and motor tube. This process is shown in Figure 11B.

Once the fin can assembly was completed, the motor mount was integrated into the sustainer tube. Prior to insertion, rings of structural epoxy were applied to the interior of the sustainer tube at the locations corresponding to the centering rings. The motor mount assembly was then inserted into the tube, with care taken to align the fins with the pre-machined fin slots in the airframe. A 6" dryer hose clamp was used to hold the assembly firmly in place during curing, ensuring proper alignment and full contact between the centering rings and the inner wall of the sustainer tube. The completed motor mount assembly and final integration into the sustainer tube are shown in Figures 11B and 11C.

This construction method results in a rigid and well-aligned propulsion structure capable of withstanding thrust and aerodynamic loads encountered during flight, while also ensuring repeatable and accurate assembly. Unlike more conventional approaches, where the motor mount is partially installed and fins are tacked individually inside the airframe, the team elected to fully assemble the fin can externally prior to insertion. This allowed the use of custom 3D-printed alignment jigs to precisely space

the fins at 90-degree intervals, improving consistency and reducing alignment error. Additionally, performing bonding and filleting operations outside of the airframe provided better access and control over epoxy application. The completed assembly could then be inserted as a single unit, preserving alignment throughout installation. This method proved to be efficient, highly replicable, and showed no compromise in structural integrity compared to traditional techniques.

E. Avionics

1. Avionics Bay

The avionics bay, located within the central coupler of the vehicle, houses all onboard electronics responsible for flight monitoring and recovery actuation. These systems determine when to initiate parachute deployment while recording telemetry such as GPS position, altitude, and battery status. The current avionics architecture consists of two Altus Metrum TeleMetrum units, a Featherweight Blue Raven altimeter, and a Featherweight GPS. The Blue Raven serves as the primary recovery flight computer, with a TeleMetrum providing redundancy. The Featherweight GPS is used as the primary tracking solution, with the TeleMetrum offering a secondary tracking capability.

In addition to the COTS systems, a Student Researched and Developed (SRAD) flight computer is being flown as an experimental tertiary system. While this SRAD board includes GPS and flight sensing capabilities, it is not used to trigger recovery events due to limited validation testing. Its inclusion allows for additional data collection and future development without introducing risk to primary mission functions.

Flight computer selection was guided by reliability, redundancy, and compatibility between systems. Following a prior recovery failure that damaged onboard electronics, emphasis was placed on selecting proven hardware with independent sensing and actuation pathways. A trade study comparing compatible flight computer pairings was conducted and is included in Appendix G-P. The selected configuration prioritizes the Blue Raven for primary deployment, supported by the TeleMetrum for fully independent backup functionality, while leveraging the Featherweight ecosystem for GPS tracking and ease of integration through its mobile interface.

All avionics systems are powered by independent 3.7V 18650 lithium-ion batteries to maintain electrical isolation and reduce the risk of common-mode failures. The TeleMetrum units and SRAD board transmit telemetry over long-range radio links, while the Featherweight GPS provides real-time position tracking. The Blue Raven, while not intended for long-range communication, enables short-range Bluetooth connectivity for post-flight data retrieval.

2. SRAD Flight Computer

The SRAD flight computer hardware has been successfully developed and tested over the spring semester. This work builds upon the SRAD hardware and firmware developed for the 2024–2025 IREC competition, pictured in Appendix G-Q. During the fall semester, the 2024–2025 design was found to have several minor issues, requiring it to be reassembled, reevaluated, and brought to full functionality. Once functionality was confirmed, the team decided to expand upon the existing design to reduce development time. Following testing of the previous board, new functionality for the 2025–2026 competition was selected, including a radio transmitter, GPS receiver, and ST-Link debugging. These

features were successfully implemented alongside existing hardware from the 2024–2025 design, including the pressure sensor, inertial measurement unit, and e-match lighting circuitry. A basic block diagram of the full system was then defined in Appendix F-O, allowing the team to proceed with schematic and PCB capture.

a. Radio Transmitter

The radio transmitter needed to be capable of sending telemetry (GPS most critically) over a line of sight distance of around 3 miles. After exploring subgigahertz transceiver IC development boards, the NUCLEO-WL55JC was selected (shown in Appendix G-R). The red boxed circuitry was used as a reference design and adapted for this application. A pair of these transmitters were tested up to ranges of 1.25 miles line of sight (the farthest practical distance able to be tested at the time), and a strong data link was maintained.

The selected transmitter reference design was modified for one way communication by removing the circuitry which supports receiver functionality, which was not required for the rocket. The package of the transceiver IC was also changed from the original reference UFBGA73 package to a UFQFPN48 which would allow for easier assembly and debugging. The final radio transmitter schematic is shown below in Appendix F-M. A completely independent transmitter microcontroller, power regulator and battery decoupled system functions independent of the main microcontroller system used for polling sensors. This design decision provides redundancy in case either of the two systems fail, either preserving telemetry logging or GPS tracking.

b. GPS Receiver

Several team members had prior experience using GPS receivers from u-blox; therefore, the SAM-M10Q and SAM-M8Q modules were compared to determine the most suitable receiver for the SRAD avionics system. The desired selection criteria included an integrated patch antenna, EEPROM logging capability, data logging support, and UART compatibility for embedded integration. The SAM-M10Q supports four GNSS constellations, including GPS, GLONASS, Galileo, and BeiDou, while offering low power consumption, high navigation sensitivity, and built-in spoofing and jamming detection. In comparison, the SAM-M8Q supports three GNSS constellations, GPS, Galileo, and GLONASS, and includes geofencing and message integrity protection, but provides slightly lower and less consistent sensitivity. Based on this comparison, the SAM-M10Q was selected for its broader GNSS support, improved sensitivity, and lower power consumption, making it more suitable for reliable SRAD GPS operation. The implementation of this receiver is shown in Appendix F-N.

c. ST-Link

ST-Link is a Serial Wire Debug (SWD) interface that allows for convenient programming and, crucially, live debugging of STM32 microcontrollers. One of the key features of this board was to implement this interface in order to improve the firmware development and testing process. Implementation of this interface required identifying the necessary pinouts on the STM32 chips and matching them to the pins of a commercial ST's V3MINIE debugger. This implementation was successful and has been extremely useful in developing firmware.

d. Testbed Board

The Testbed board is an intentionally oversized version of the complete avionics system design, developed to simplify assembly, troubleshooting, and firmware development. It includes numerous test points and widely spaced components that provide easier probe access during testing, many of which will be removed from the final flight board to reduce board size and meet avionics bay constraints. The board has been successfully assembled and tested and is currently being used for flight firmware development, as shown in Figure 12. As a contingency measure, mounting holes for the Testbed board have also been incorporated into the avionics bay, allowing it to be flown in place of the flight-form-factor board if necessary.

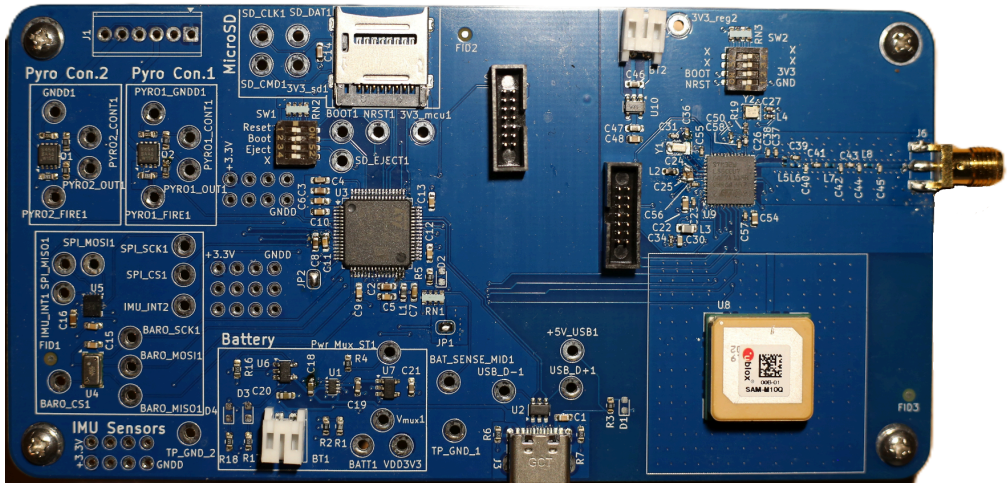


Fig 12: SRAD Testbed Board

e. SRAD Testbed Flight Computer Results

All sensors and telemetry have been verified on the Testbed board. Shown in Appendix G-S and G-T, data saved on the Testbed board SD card was plotted, showing accelerometer and pressure sensor functionality. Appendix G-U shows live GPS telemetry that was plotted on mapping software called OpenCPN.

f. Final Flight Form-Factor Board

The final flight form-factor SRAD flight computer, shown in Appendix G-V, represents an evolution of the Testbed design with an emphasis on manufacturability, reliability, and avionics bay integration. While the core architecture and functionality remain largely unchanged from the testbed board, the final board incorporates several refinements to better prepare the system for flight. The overall board dimensions were adjusted to improve fitment within the avionics bay, and the GPS receiver was relocated to the reverse side of the board to provide a larger uninterrupted ground plane in the receiver's vicinity, aligning with manufacturer recommendations for improved performance. Additional footprint corrections and layout optimizations were also made based on issues identified in the testbed version. Finally, an RF shield was added over the radio transmitter and associated circuitry to help mitigate external electromagnetic interference.

F. Recovery Subsystems

1. Overview

The recovery subsystem is responsible for safely decelerating and returning the vehicle while minimizing risk to personnel, equipment, and the airframe. As a safety-critical system, the design prioritizes reliability, redundancy, and controlled deployment over performance optimization, as failure would result in total vehicle loss.

The vehicle employs a dual-separation, dual-deploy architecture, with a drogue parachute deployed at apogee and a main parachute deployed at low altitude. This approach reduces drift during early descent while ensuring a low terminal landing velocity. Independent separation events are used for each deployment to improve fault tolerance and reduce failure coupling (see Figure 15 for CONOPS).

Recovery events are initiated using black powder charges triggered by redundant avionics. Primary and secondary charges at each separation point are controlled by independent flight computers, providing redundancy in both sensing and actuation. Physically independent charge wells and wiring paths further reduce the risk of common-mode failures.

Structural components, including bulkheads, attachment hardware, and shock cords, are designed to withstand dynamic deployment loads using conservative margins. Preliminary sizing is supported by analytical calculations, with final validation planned through finite element analysis and ground-based testing. Together, these elements form a robust recovery architecture designed to provide reliable and repeatable performance under nominal and off-nominal conditions

2. Black Powder Charges & Charge Wells

Black powder ejection charges are used to initiate the rocket's recovery separation events. Charge wells contain the measured black powder charge, isolate the energetic event from surrounding avionics and recovery hardware, and promote consistent pressure generation for reliable deployment. Primary and redundant backup charges are used at each separation event to support the dual-deploy recovery architecture.

For the 2026 vehicle, the charge wells were redesigned to include an internal e-match channel that routes the igniter to the top of the black powder volume. Previous charge wells ignited from the bottom, which could expel unburned powder before complete combustion, reducing pressure generation at altitude. The new top-down ignition path promotes more complete combustion and improves separation reliability. Due to the new internal channel, the charge wells could not be manufactured using traditional subtractive techniques, making metal additive manufacturing the preferred fabrication method.

The charge wells were printed from Inconel 718 using a Selective Laser Melting (SLM) metal printer at Rowan University's Digital Engineering Hub. Inconel was selected for its strength, fracture toughness, fatigue resistance, and ability to withstand transient pressure spikes from black powder deflagration. After printing, the parts were annealed to reduce hardness and allow post-processing. The external M18×1.5 threads were then machined using a tap to ensure proper fit with the avionics bay bulkheads.

The final design, demonstrated in Figure 13, maintains Rowan Rocketry's recessed charge well configuration, where each charge well threads into the avionics bay bulkhead from the inside rather than protruding externally. This protects the wells, preserves a clean exterior bulkhead face, and continues a design approach used successfully on prior Rowan vehicles. The resulting charge wells provide a durable, reusable, and high-temperature-capable solution for recovery deployment.

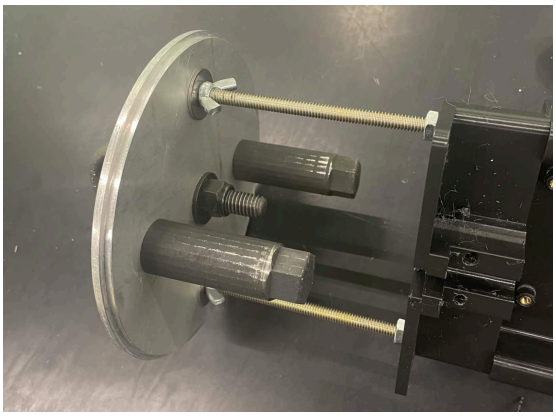


Fig 13: Charge Well Assembly

3. Parachute Configuration

The recovery system uses a dual-deploy configuration with a 3 ft drogue parachute at apogee and a 14 ft main parachute at low altitude, enabling a fast, stable descent under drogue to minimize drift followed by a low terminal velocity for safe landing. Parachute sizing was determined through trade studies evaluating descent rate, landing velocity, and deployment loads, which can be seen in Appendix G-W. A 3 ft elliptical drogue was selected to maintain a controlled high-rate descent without introducing excessive loads, while the 14 ft Rocketman Iris Ultra main parachute provided the best balance between low landing velocity and acceptable snatch force. Simulations predict a landing velocity of approximately 9 ft/s and a main-deployment snatch force of 1,200–1,300 lbf, both within structural limits. Larger parachutes were evaluated but produced significantly higher snatch forces with minimal improvement in landing performance. This year, the team is also implementing protective blankets for all recovery components, replacing the previous reliance on parachute bags without pilot chutes. The blankets simplify packing, shield the canopies from ejection gases, and are expected to improve deployment consistency and canopy inflation reliability. A comprehensive illustration showing all recovery stages can be found in Appendix G-X.

4. Bulkhead Structural Analysis (FEA)

The design of our bulkheads is similar to previous years, with some small modifications to fit the dimensions of this year's rocket body. In order to ensure that the bulkhead design would withstand the expected forces during flight, we performed finite element analysis simulations using Solidworks. The main force that will be applied to the bulkheads will be the snatch force from the opening of the parachutes. For this, the main parachute was primarily analyzed, as it will have a significantly larger snatch force than the drogue chute. Our calculations indicate that the maximum snatch force that may be

experienced upon parachute deployment is 1,267 lbf, and are supported by the calculations shown in Appendix G-Y.

This value will likely not be fully realized during flight, as this assumes that the main parachute opens instantaneously, an unrealistic assumption. However, our finite element analysis calculations still use a value of 1,250 lbf, as all operating loads will be bounded above by this value.

From our finite element analysis simulations, our middle bulkheads have a factor of safety (FOS) of approximately 1.6, and our outer bulkheads have a FOS of about 1.7 (Appendix G-Z, G-AA, G-AB). These values indicate that, in a worst case scenario, our bulkheads still have available safety margin and are at no risk of failure.

G. Telemetry

1. Telemetry Scenario

Our avionics bay will be transmitting on the 70cm band and the 33cm band. In total, the system will transmit over three different frequencies: one in the 70cm band for the Altus Metrum Telemetrum, one in the 70cm band for our SRAD computer, and one in the 33cm band for our Featherweight GPS. The Telemetrum will be transmitting information including GPS coordinates, battery voltage, flight state, barometric altitude, velocity, acceleration, pyro channel continuity, and signal strength. The Featherweight GPS will be transmitting information, including GPS coordinates and velocity derived from the GPS coordinates.

2. Ground Station

The ground station consists of a manually directed 70 cm Yagi antenna for the TeleMetrum system, a semi-autonomous 70 cm Yagi antenna tracker for the SRAD flight computer, and a handheld Featherweight GPS receiver linked to a smartphone. The Featherweight GPS provides a map interface showing the rocket's location, bearing, and distance from the ground station, while the TeleMetrum and SRAD systems provide additional telemetry and tracking capability.

The semi-autonomous tracking system, referred to as the Turret, was developed to reduce the number of operators required to maintain antenna alignment during flight. The system uses a handheld Commander module containing an ESP32 microcontroller and inertial measurement unit to measure the operator's pointing direction. This orientation data is transmitted wirelessly to a second ESP32 within the Turret, which commands the mechanical pointing system to match the operator's azimuth and elevation. A CAD rendering of the Turret assembly is shown in Figure 14.

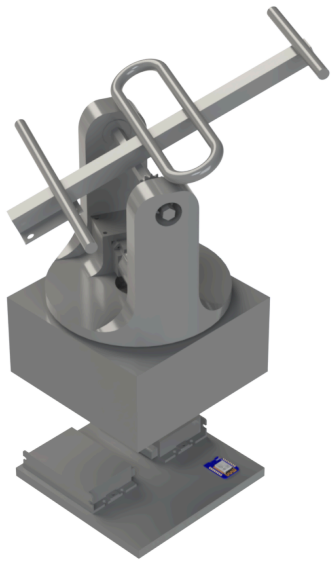


Fig 14: Ground Station CAD

For this competition year, the Turret will operate as a human-guided pointing aid rather than a fully autonomous tracking system. This implementation validates the mechanical structure, wireless communication architecture, embedded control hardware, and antenna mounting approach. Future development may replace operator-generated pointing data with GPS-derived rocket position data from the SRAD flight computer, enabling autonomous antenna tracking.

In accordance with current competition rules and Student Band Plan guidance, the team is prepared to select assigned 70 cm operating frequencies for the SRAD and TeleMetrum systems, while the Featherweight GPS will operate on an assigned 33 cm frequency. Additional ground support equipment includes a custom Pelican-style field case to house the laptop and supporting hardware while protecting the system during launch operations.

H. Payload Subsystems

1. Overview

The payload is a self-contained, 10 cm x 10 cm x 30 cm box that houses the electronic components. The purpose of this payload is to monitor ambient temperature/observe changes, and it includes electronics to measure temperature, altitude, and pressure. The box itself must weigh at least 4.4 lbs (2kg) to be eligible for the competition. These limitations required careful planning of material selection, assembly, and electronic placement to achieve the most accurate results with the least interference.

2. Design

The payload consists of an aluminum inner box and outer box with a layer of insulation between them. Aluminum was chosen as the material because of its affordability, high melting point, and ease of

use. The boxes are held in place in the rocket via a payload holder. The outer box is ⅛", and the inside is .09 "of aluminum. The insulation used was Great Stuff Pro Plus because it was affordable and obtainable within our budget. The panels are held together with screws, and the electronics are mounted on the inner box's sum plate. This is done by putting holes into the inner box and screwing the protoboard with the electronic devices on it. The protoboard is mounted to standoffs to keep it off the aluminum inner box and prevent any possible conductivity. Strong magnets are used to keep the outer door shut and to contain the payload's contents. One consideration when creating the payload was the effects heat transfer had on the payload and the electronics inside. Keeping the temperature below 80°C during launch was a main concern for the electronics, as anything above that could cause them to malfunction and yield false results. Placement of these components also mattered, as there was little space, and they needed to be somewhere where all the parts would stay in place. All electrical connections are insulated with heat-shrink tubing, and wiring is secured to prevent movement or short circuits during flight.

3. Electronics

Located in the inner box of the payload are a 7x3 cm protoboard, an Arduino Nano Every microcontroller, a BMP280 temperature/pressure sensor, 3 AA batteries, and a battery holder. Code that sends bits to the microcontroller enables the BMP280 sensor to send data, including pressure and temperature, back to the Arduino. The objective is to better understand how these factors affect astronauts' function and nervous systems. This system is non-deployable and is meant to stay inside the rocket until landing. After landing, and the electronics are recovered, can the data be retrieved and observed. The payload is a non-deployable, self-contained system that remains enclosed in the payload bay throughout flight and recovery. Despite being non-deployable, it is designed to be fully removable from the launch vehicle for independent weighing and inspection, in compliance with IREC requirements. This allows both the recovery and payload systems to be recovered simultaneously and easily. Data is logged on board and retrieved post-flight via a direct connection to the microcontroller.

I. No other subsystems that are flight-critical were used.

IV. Mission Concept of Operations Overview (CONOPS)

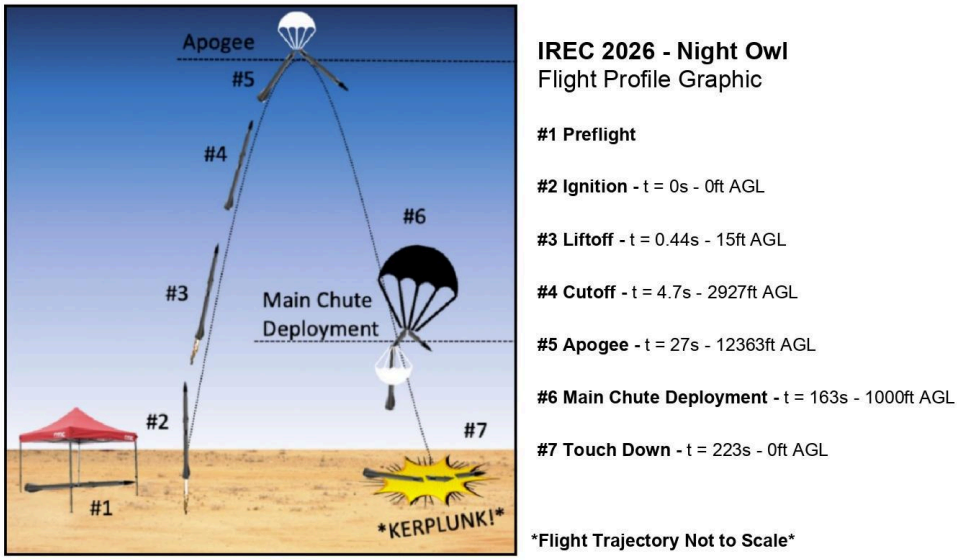


Fig 15: Night Owl Mission Profile

Night Owl's nominal mission is divided into seven phases, beginning with preflight preparation and ending with post-touchdown recovery. These phases define the expected propulsion, avionics, recovery, and telemetry events throughout flight. During preflight, the vehicle is prepared on the pad, the motor and ignition system are secured, and the recovery electronics are powered and armed. After ignition, the motor produces thrust, the vehicle lifts off the rail, and powered ascent continues until burnout. The rocket then coasts to apogee, where avionics command drogue deployment. At the selected altitude, the main parachute deploys for safe landing, while telemetry supports tracking and recovery.

A. Definitions

Table 1: Definitions of Control Systems

Subsystem	Abbreviation	Function
Flight Propulsion System	FPS	Solid rocket motor that produces thrust during powered ascent
Propulsion Ignition System	PIS	Starter and launch command system used to initiate motor ignition
Vehicle Recovery System	VRS	Flight computers, parachutes, ejection charges, and GPS used for descent and recovery
Mechanical Safe	MS	Physical safing device, such as screw switches
Software Safe	SS	Digital command or software state used to prevent unintended activation

B. Mission Phases

Table 2: Mission Phase and Subsystem Operations Matrix

Phase	Mission Event/Transition	Propulsion/Ignition	Recovery	Avionics/Telemetry
1. Preflight	Vehicle is on pad and prepared for launch	Motor installed and secured; ignition system safed until launch command	Drogue and main parachutes packed; ejections charges installed and unfired	Flight computers, GPS, and telemetry powered; recovery system armed
2. Ignition	Launch command activates starter and motor begins combustion	Ignition system activated; motor pressurizes and begins producing thrust	Recovery system remains armed with charges unfired	Flight computers record launch conditions; telemetry remains active
3. Liftoff	Vehicle begins motion and clears the launch rail	Motor actively produces thrust during powered ascent	Drogue and main remain internal; charges unfired	Avionics monitor acceleration, altitude, and flight state
4. Cutoff	Motor burnout occurs and thrust ends	Motor is consumed; vehicle enters unpowered coast	Recovery system remains armed; charges unfired	Avionics continue tracking altitude and acceleration as vehicle approaches apogee
5. Apogee	Vehicle reaches apogee and begins descent	Propulsion systems inactive	Drogue deployment charges fire; airframe separates and drogue deploys	Flight computers detect apogee and command drogue deployment
6. Main Deploy	Vehicle descends to main parachute deployment altitude	Propulsion systems inactive	Main deployment charges fire; main parachute deploys	Flight computers detect deployment altitude and command main deployment
7. Touchdown	Vehicle impacts ground at low velocity	Propulsion systems inactive	Drogue and main parachutes inactive after landing; charges expended	Telemetry supports vehicle location and recovery

V. Conclusion

This year's vehicle demonstrates significant growth in the team's engineering discipline, marked by a shift toward rigorous analysis, structured decision-making, and improved subsystem integration. The project reflects a maturing systems-engineering approach that balances analytical tools, practical constraints, and lessons learned from prior years.

A. Team Management Lessons

The adoption of structured collaboration tools: Google Drive for documentation, GitHub for version control, and formal decision frameworks such as QFD and FMECA, improved traceability and communication across subsystems. These methods increased transparency and reduced ambiguity in design choices, though they also highlighted the need for clearer data-management practices and more deliberate coordination during high-workload periods. The team learned that consistent documentation, early alignment on interfaces, and regular cross-subsystem reviews are essential for maintaining schedule discipline and avoiding integration bottlenecks.

B. Technical Lessons

Expanded use of analytical tools such as OpenRocket, RASAero, MATLAB, and finite element analysis improved understanding of system behavior prior to fabrication, but also underscored the sensitivity of simulations to assumptions about materials, environment, and manufacturing tolerances. The team learned to treat analytical outputs as guidance rather than absolute predictions, applying conservative margins to account for uncertainty. Manufacturing and integration efforts reinforced the importance of designing within available resources, validating assumptions through testing, and prioritizing reliability over unnecessary complexity.

C. Strategies for Knowledge Transfer

Sustaining progress across academic years requires deliberate knowledge-transfer practices. This year emphasized maintaining organized design repositories, documenting subsystem decisions and rationale, and standardizing testing procedures to reduce onboarding time for new members. Clear subsystem handoff documents, updated CAD and simulation libraries, and consistent use of shared digital platforms will enable future teams to build on established work rather than restarting design efforts. These strategies ensure continuity, preserve institutional knowledge, and support long-term program growth.

VI. Appendix A

Systems Weights, Measures and Performance Data

Table A-A: Basic Rocket Vehicle Information

Parameter	Value
Number of stages	1
Length	1.3716 m
Airframe diameter	156.718 mm
Number of Fins	4
Fin semi-span	6.5"
Fin tip cord	4"
Fin root cord	16"
Fin thickness	0.1875"
Weight on launch rail	60.6 lb
Propellant weight	5368 g
Empty motor case/structure weight	40.7 lb
Payload Class	Attached CubeSat
Payload weight	2 kg
Liftoff weight	60.6 lb
Center of pressure	70.491"
Center of gravity	82.356"
Launch rail length	12'

Table A-B: Propulsion Information

Parameter	Value
Motor type	Solid
Whether it is COTS or SRAD	COTS
COTS manufacturer and designation	AeroTech M2000R
Average thrust (N)	2000.0 N
Total Impulse (Ns)	9218.0 N
Motor burn time	4.0 s

Table A-C: Predicted Flight Data

Parameter	Value
Liftoff thrust-weight ratio (X:1)	10.7:1
Rail departure velocity	26.3 m/s
Minimum static margin	10.50%
Maximum acceleration (G)	8.95 G
Maximum velocity	324 m/s
Fin flutter velocity	722 m/s
Target apogee	3048 m (10000 ft)
Predicted apogee	3581 m

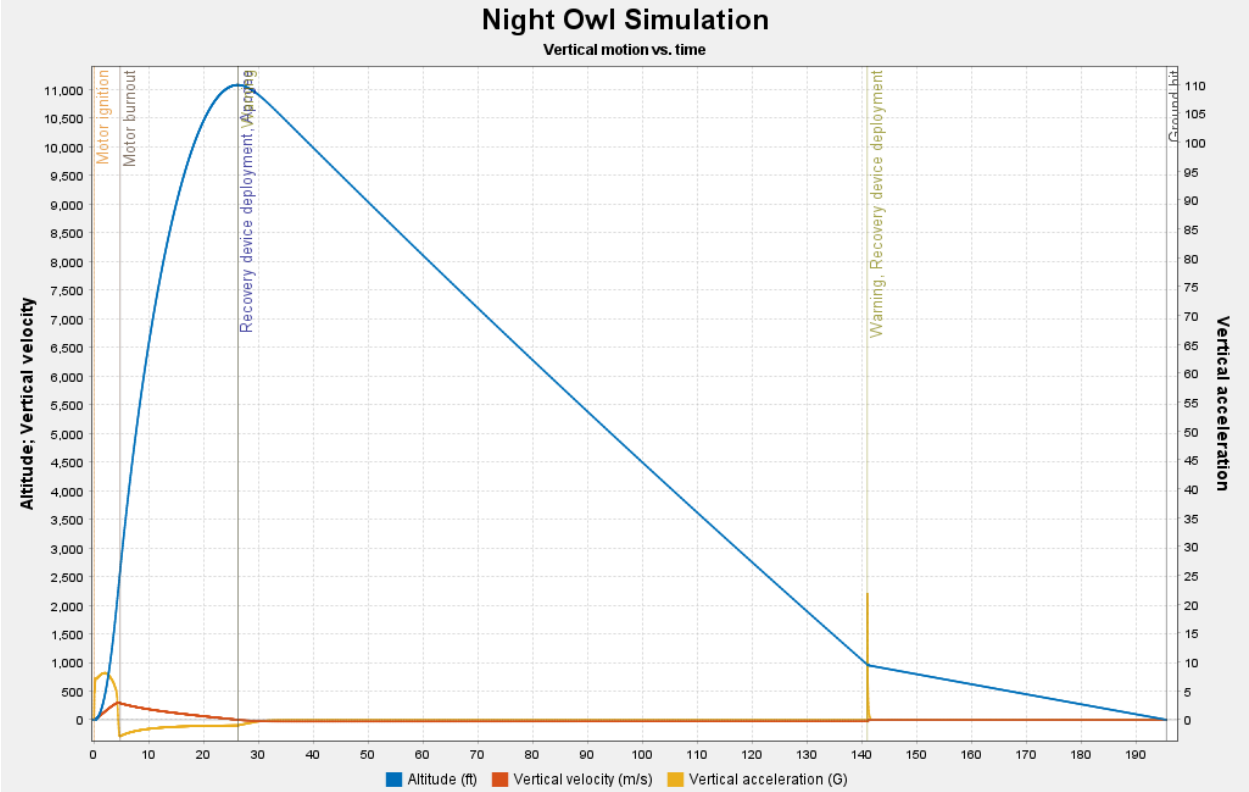


Figure A-D: Flight Profile Graph

Table A-D.1: Basic Recovery Information

Parameter	Value
Primary Altimeter	Featherweight Blue Raven
Backup Altimeter	Altus Metrum Telemetrum
Live Telemetry	Yagi Antenna
Tracking	Featherweight Blue altimeter, Altus Metrum TeleMetrum
Shear Pins	4-40 Nylon Screws
Shock Chord/Harnesses	30 ft nylon
Linkages	3000 lb quick links
Connection Point Type	Eye Bolts
Deployment Charge Powder	4F Black Powder

Table A-D.2: Drogue Parachute Information

Parameter	**Value**
Chute Type	Rocketman 3' Experimental Drogue
Protection	24"x24" Nomex Blanket
Primary Deployment Charge	3g Black Powder Charge
Backup Deployment Charge	4g Black Powder Charge
Deployment Altitude	Apogee
Descent Rate	-27.24 m/s

Table A-D.3: Main Parachute Information

Parameter	Value
Chute Type	Rocketman 14' Elliptical
Protection	24"x24" Nomex Blanket
Primary Deployment Charge	3g Black Powder Charge
Backup Deployment Charge	4g Black Powder Charge
Deployment Altitude	1000' AGL
Descent Rate	-5.32 m/s

VII. Appendix B

Project Test Reports

Night Owl Ground Test Report

Date: 4/14/2026
Situation: Test
Result: Pass/Fail
Reporter: Paul Porreca

Summary:
Deployment Test Using Primary Chargewells

Objectives:
Test Recovery with rocket in full flight configuration form
Sustainer separation/main deployment
After Nosecone separation/drogue deployment

Notable System Changes: N/A

MATERIALS CHECKLIST

Chutes:	**Ejection Canister:**
X Shock Cord Systems	X Chargewells (x2)
X Main	X Powder
X Main Bag	X E-Matches (x2)
X Drogue	
X Drogue Blanked	

CHARGES

E-Matches:

Powder:
Type of Powder: 4F Black Powder
Amount Used in Ejection Canister: 3 grams

SYSTEM

Current Weight of Nosecone: 9.2 lbs
Sheer Pins Used: 4

NOTES

Successful test overall: good separation and deployment

Night Owl Ground Test Report

Date: 4/30/2026
Situation: Test
Result: Pass/Fail
Reporter: Paul Porreca

Summary:
Fully Integrated Deployment Test

Objectives:
Test Recovery with rocket in full flight configuration form
Sustainer separation/main deployment
After Nosecone separation/drogue deployment

Notable System Changes: N/A

MATERIALS CHECKLIST

Chutes:	**Ejection Canister:**
X Shock Cord Systems	X Chargewells (x4)
X Main	X Powder
X Main Bag	X E-Matches (x4)
X Drogue	
X Drogue Blanked	

CHARGES

E-Matches:

Powder:
Type of Powder: 4F Black Powder
Amount Used in Ejection Canister: 4 grams

SYSTEM

Current Weight of Nosecone: 9.2 lbs
Sheer Pins Used: 4

NOTES:

Successful test overall: good separation and deployment

VIII. Appendix C

Hazard Analysis

Combustible Product Hazard: Redline 8125RC Propellant

Redline 8125RC is an AeroTech ammonium perchlorate composite propellant (APCP) that is commonly used in high power rocketry. Ammonium Perchlorate poses serious safety risks if handled improperly. Rowan Rocketry currently stores all hazardous materials in a locked containment vessel in a temperature controlled environment.

The thermal decomposition of ammonium perchlorate occurs between roughly 130-150 [℃] (Reference). While it is not a concern that the rocket will reach this temperature even under extended exposure to solar radiation and elevated environmental temperatures, extra safety precautions are taken to ensure proper handling of Redline 8125RC Propellant. During transportation propellant will be stored in a locked, water-proof, and non-conductive containment vessel, in a temperature controlled vehicle, to avoid unnecessary risk.

Combustible Product Hazard: Black Powder

4F black powder is a combustible product that is used in the ejection charge wells and detonated to create pressure in the recovery bays. This pressure is harnessed to separate the rocket and deploy the parachutes. This introduces a hazard during the packing of the recovery bays, transportation of said black powder, and arming the charges.

1. *Transportation*

The black powder is transported and stored in a plastic bottle with a threaded-on cap. That bottle is then stored in a sealed, non-conductive box for use when transporting the powder in vehicles and at the launch site.

2. *Storage*

The black powder is stored in the aforementioned plastic container. It will be stored in a cool-to-room-temperature cabinet away from any combustible items, heat sources, or electrical components (batteries, etc). During recovery preparation, the powder is measured from the plastic container, then the lid is secured, and the container is returned to its safe location.

3. *Handling*

During assembly of the ejection charges, the e-match wires are kept clipped so the leads remain insulated and not exposed to any potential static charge in the surrounding environment. While installing the charges, the e-match leads are connected to the e-bay using insulated connections to prevent contact with the airframe and reduce the risk of unintended discharge. All power is disconnected before making any connections. Ejection charges are only prepared on the day of testing by a team member experienced in handling black powder, under the supervision of a faculty advisor.

IX. Appendix D

Risk Assessment

* Likelihood (L) of instance to occur; ranked 1 = least likely & 10 = most likely

** Severity (S) of the risk's impacts; ranked 1 = not severe & 10 = extremely severe

*** Mission Phase (MP): 0 (Manufacturing & Assembly); 1 (Before launch); 2 (At launch); 3 (Ascension); 4 (Apogee); 5 (Descension); 6 (Landing)

MP	Risk	Possible Causes	Mitigation	L	S
0	Injury during fabrication	Inhalation of epoxy fumes, Sharp edges, Improper use of tools/machinery	Follow all workshop and other relevant safety protocols and have experienced users operate more dangerous machinery.	3	8
0	Inability to assemble rocket	Lack of fasteners and other hardware, Damage to components during transportation	Bring extra hardware, Pack and secure components properly during travel	2	5
0	Fabrication failure	User error, improper tool use, failure to verify successful fabrication	Have multiple people check blueprints and fabrication plans, verify components fabricated successfully	5	4
1	Electronics general failure	Wire issues, Battery malfunction, Short circuit	Thorough testing and following premade avionics flight operations checklist	4	4
2	After ignition command motor does not engage	Starter failure	Ensure starter successfully fires, bring additional starters	3	1
2	Motor assembly becomes unaligned	Improperly secured motor casing or centering rings	Proper preassembly to ensure structural design and checking before launch	3	6
3	E-match switches triggers prematurely	Bad sensor data causes early E-match ignition	Thorough sensor testing	3	5
3	Failure to launch straight off launch rail	Insufficient thrust, misaligned rail buttons	Test computer and launch rail compatibility	3	6
3	Body tube failure	Improper fabrication, epoxy failure	Ensure proper fabrication and double check finished project, Keep out of harsh conditions	2	7
3	Premature rocket separation	Weak or not enough shear pins	Test launch and perform evaluation on shear pins	1	8
3	Fin failure	Fin flutter, improper fabrication	Extensive analysis and testing of fins	3	7

4	Data logging failure	Individual sensor fails, causing software to hang	Redundant sensors across three flight computers prevent any one sensor from preventing data logging. Software timeouts to prevent software from hanging.	2	4
4	E-match switch fails to trigger	Failure to detect apogee, bad E-match	Redundant e-match switches exist across multiple flight computers. Continuity testing of matches prior to installation	4	7
4/5	Rocket tube fails to seperate	Flight computer malfunction, Charge Well malfunction	Extensive ground tests for rocket separation	3	8
5	Drogue and main parachute fail to deploy properly	Tangled shock cord/blanket, Eyebolt/Shockcord detachment	Ensure proper folding and storage of parachute, Analysis of eyebolts and shock cords to ensure necessary strength	3	8
6	Injury to people or destruction of property on landing	Improper alignment of launch tower, premature main parachute deployment	Ensure proper procedures are followed in setting up launch tower and double check, Perform ground tests and ensure parachute is properly packed	2	7
6	Damage to rocket on landing	Wrongly sized parachutes, landing on poor terrain	Ensure proper analysis of size of parachutes needed, Remain aware of winds to prevent drift outside of planned landing area	3	5
6	GPS telemetry lost	Signal attenuation over distance causes loss of signal	Range testing and RSSI extrapolation	3	4
3	Microcontroller stops working during flight	Vibration during launch or power interruption	Secure mounting, vibration damping, pre-flight power check	4	9
3	Sensor provides incorrect readings or fails	Electrical noise, loose wiring, or calibration drift	Secure soldered connections, pre-flight calibration check	5	7
4	Battery dies mid-flight	Insufficient capacity or poor connection	Fully charge before launch, test discharge duration	3	10
3	Heat leaks into cabin	Gaps in insulation or imperfect sealing	Ensure tight assembly, verify insulation coverage	4	6
4	Wire disconnects during launch	Vibration and poor strain relief	Use secured connectors and hot glue/strain relief	6	8

X. Appendix E

Assembly, Preflight, Launch, and Recovery Checklists

1. Pre-Launch Assembly Checklist

Airframe & Structures

☐ All body tube sections inspected for cracks, delamination, or damage
☐ Couplers and joints properly bonded and secured
☐ Nose cone securely attached and seated
☐ Fin alignment verified (no visible misalignment or looseness)
☐ Boat tail installed and locked (set screw secured)

Propulsion

☐ Motor casing inspected and assembled per manufacturer spec
☐ Motor retention system (Aeropack) secured
☐ Igniter installed and leads protected
☐ Motor fully seated in motor mount

Recovery System

☐ Drogue parachute packed and secured
☐ Main parachute packed and secured
☐ Shock cords inspected (no fraying or wear)
☐ All quick links tightened and secured
☐ Shear pins installed (correct quantity and size)

Avionics

☐ Flight computers (Blue Raven + EasyMini) installed
☐ Batteries charged and connected
☐ Wiring secured and strain-relieved
☐ GPS module installed and antenna unobstructed
☐ Switch band accessible and functional

Payload

☐ Payload secured in holder
☐ Sensors powered and logging
☐ Payload mass verified ≥ 4.4 lb requirement

2. Avionics & Electrical Checklist

- ☐ Altimeters powered on
- ☐ Proper startup tones/beeps confirmed
- ☐ Continuity confirmed for:
- ☐ Drogue charge
- ☐ Main charge
- ☐ Flight mode configured correctly
- ☐ Main deployment altitude set
- ☐ GPS signal acquired and transmitting
- ☐ Data logging enabled
- ☐ Backup altimeter functioning independently

3. Pyrotechnics & Recovery Charges Checklist

- ☐ Charge wells filled with correct BP mass
- ☐ Charges measured and recorded (g)
- ☐ E-matches properly installed and secured
- ☐ Charge wells sealed and protected
- ☐ Wiring continuity verified
- ☐ Ground testing previously validated configuration
- ☐ Redundant deployment paths verified

4. Launch Pad Checklist

- ☐ Rocket transported safely to pad
- ☐ Rail buttons aligned and engaged
- ☐ Igniter connected to launch system
- ☐ Final continuity check passed
- ☐ Range Safety Officer (RSO) approval received
- ☐ Weather conditions within acceptable limits
- ☐ Launch area cleared

5. Post-Flight Checklist

- ☐ Visual tracking maintained during flight
- ☐ GPS location acquired
- ☐ Rocket located and recovered
- ☐ All components accounted for:
- ☐ Nose cone
- ☐ Payload
- ☐ Avionics bay
- ☐ Recovery components

- ☐ Damage inspection performed
- ☐ Flight data downloaded
- ☐ Anomalies documented

6. Safety & Compliance Checklist

- ☐ Payload meets mass requirement (≥ 4.4 lb)
- ☐ No prohibited materials used
- ☐ Electrical systems isolated until launch
- ☐ Proper PPE used during assembly
- ☐ Safe handling of black powder charges
- ☐ Rocket complies with Tripoli / IREC safety standards
- ☐ Documentation ready for judges

XI. Appendix F

Engineering Drawings

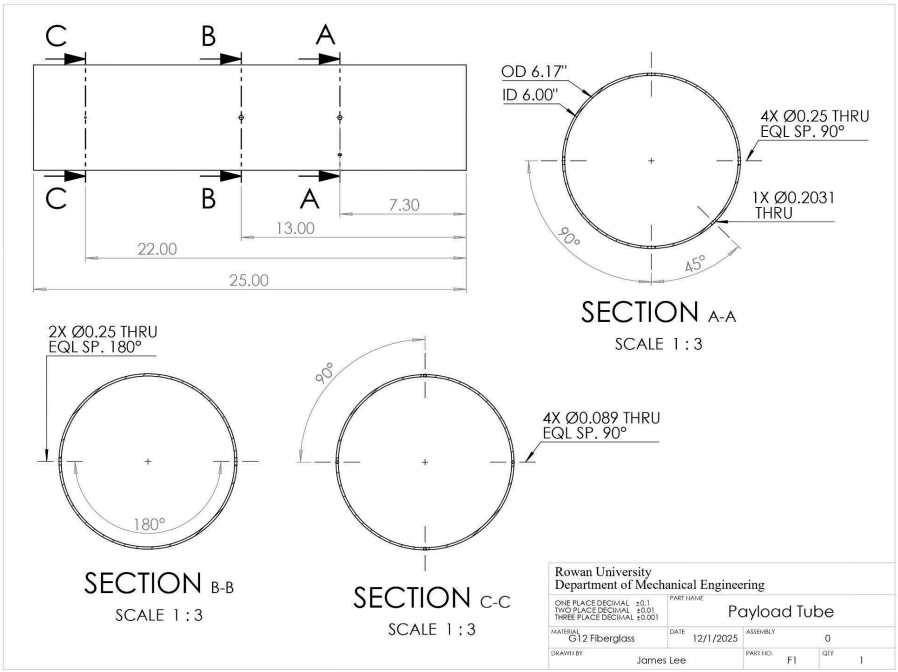


Figure F-A. Payload Tube Drawing

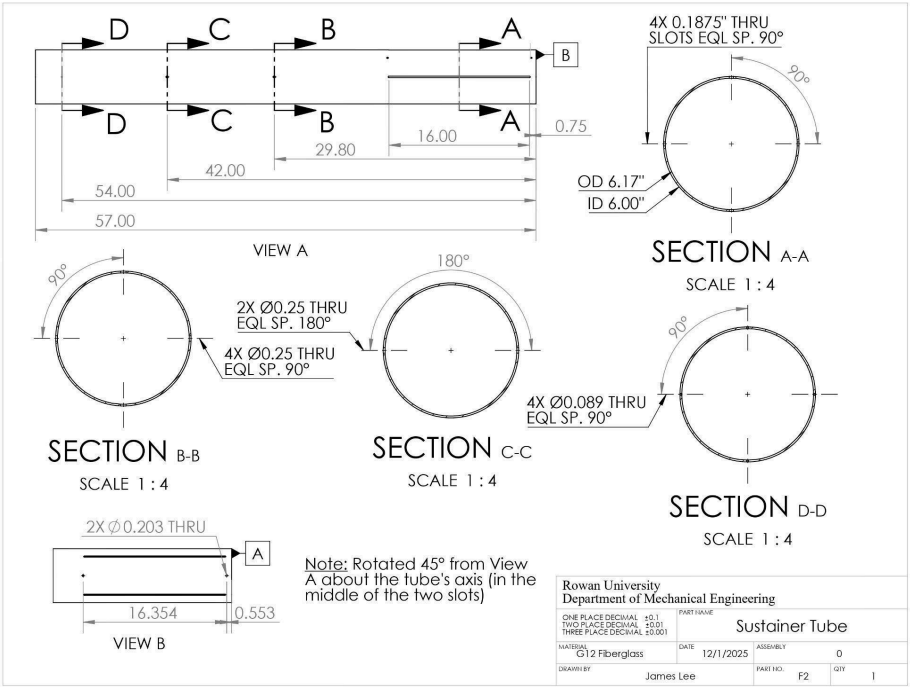


Figure F-B. Sustainer Tube Drawing

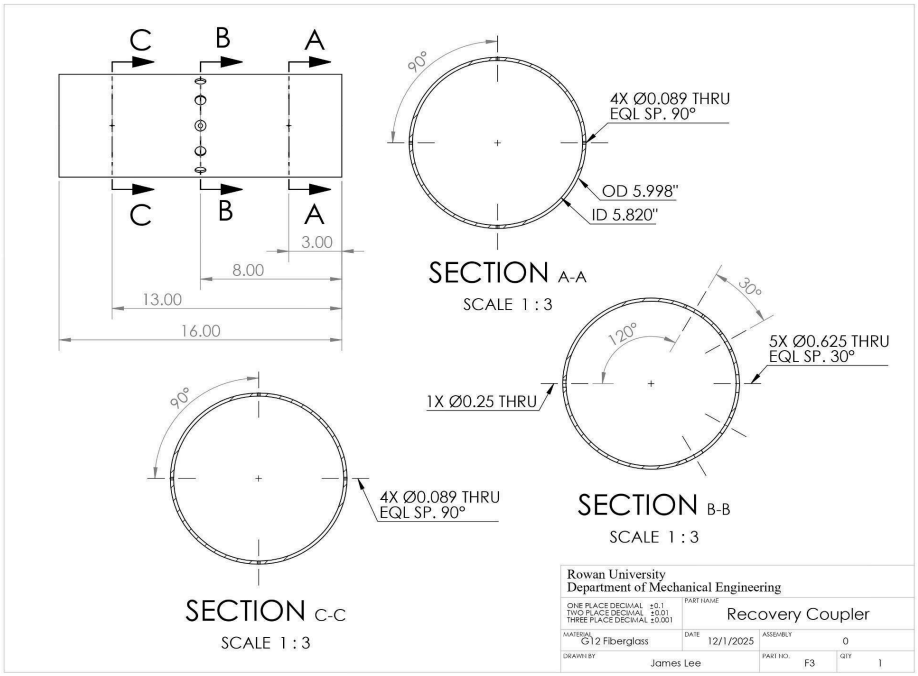


Figure F-C. Recovery Coupler Drawing

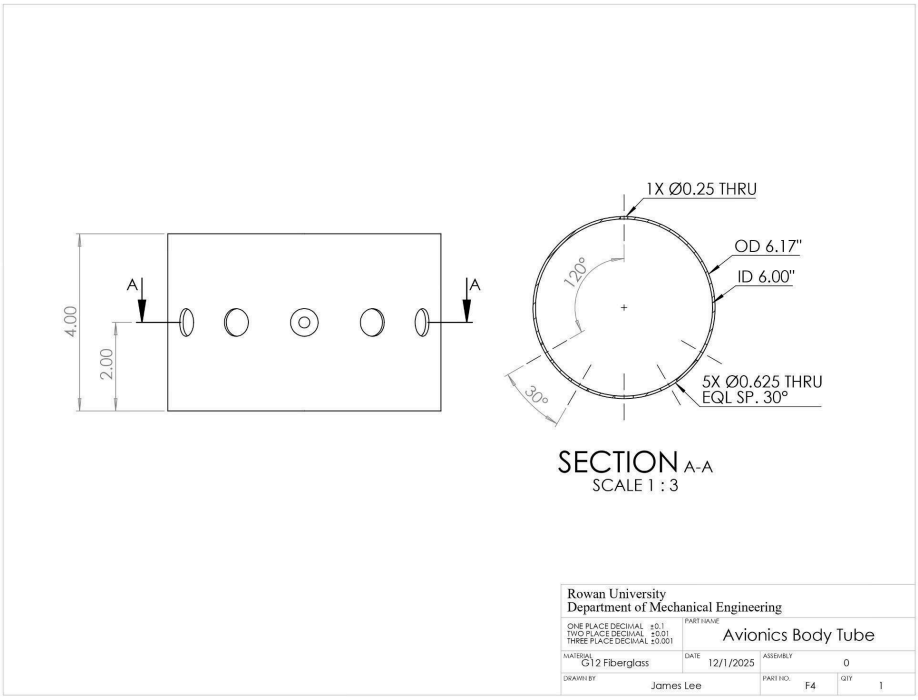


Figure F-D. Avionics Body Tube Drawing

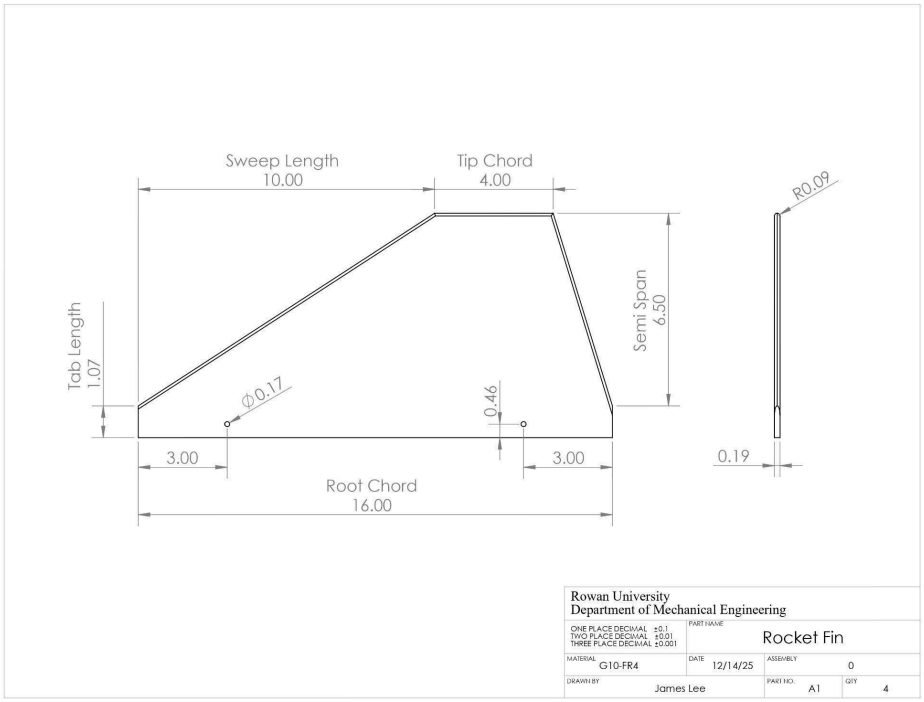


Figure F-E. Rocket Fin Drawing

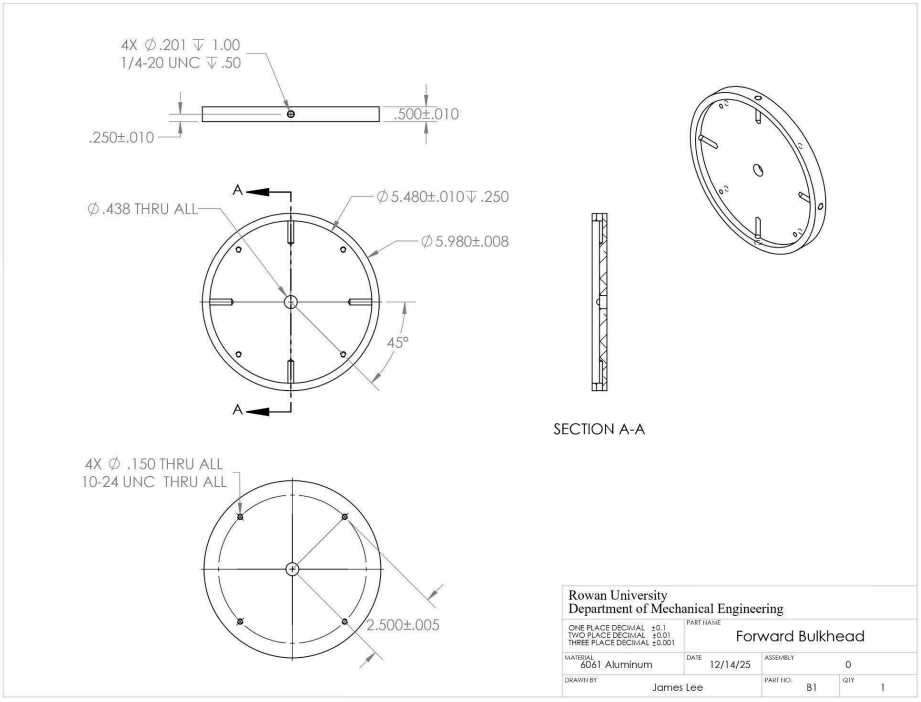


Figure F-G. Forward Bulkhead Drawing

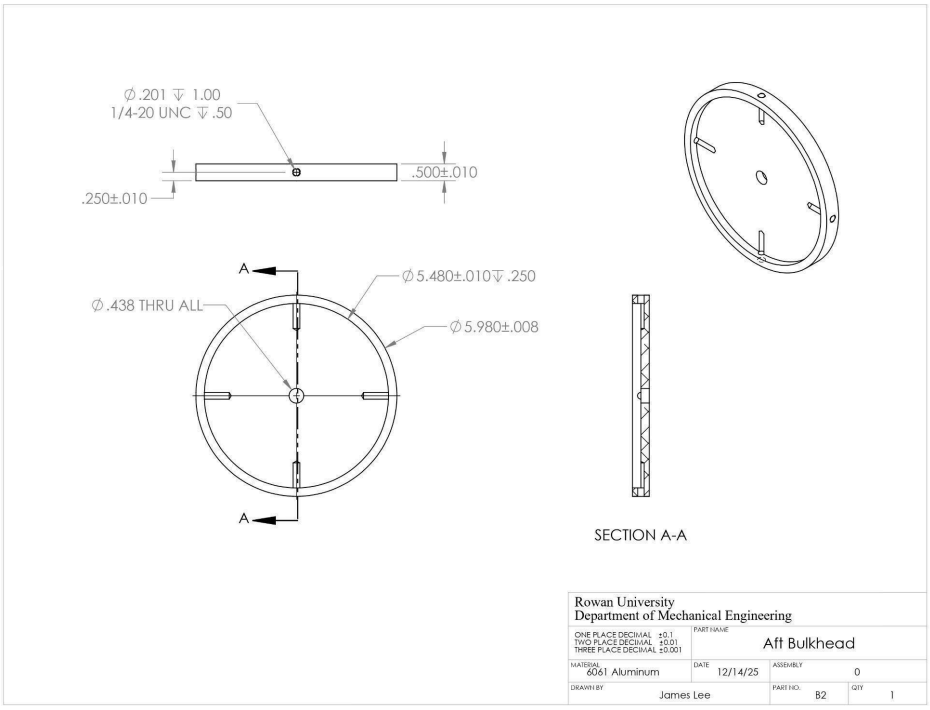


Figure F-H. Aft Bulkhead Drawing

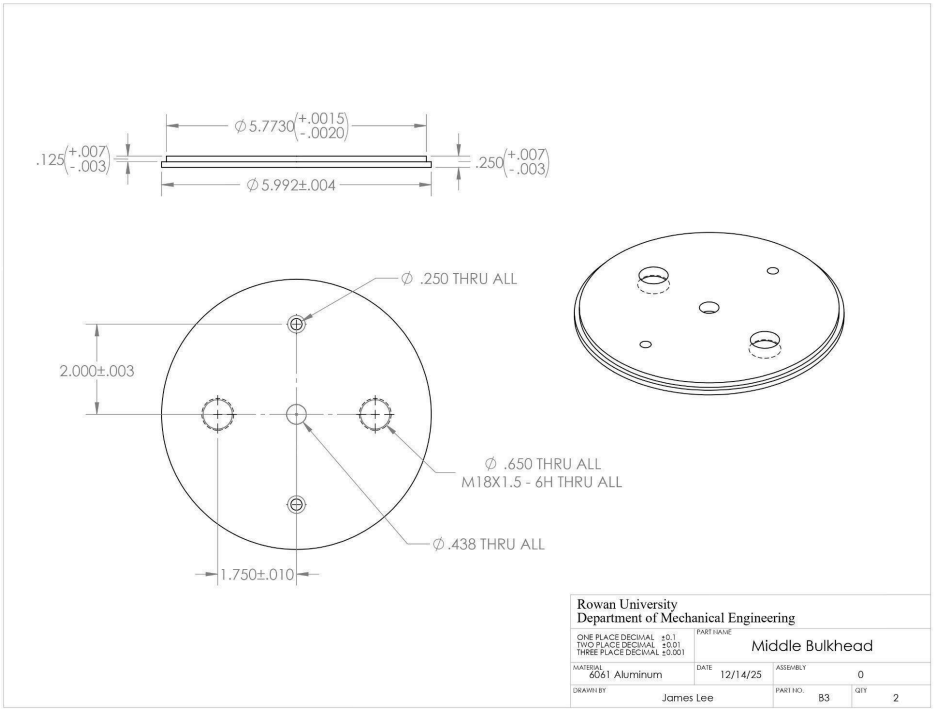


Figure F-I. Middle Bulkhead Drawing

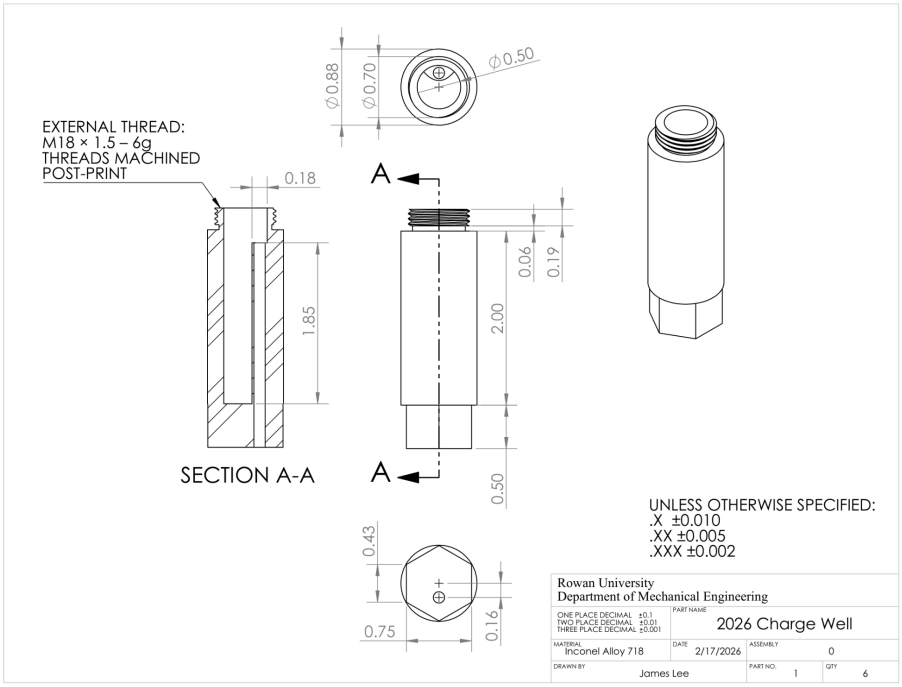


Figure F-J. Forward Centering Ring Drawing

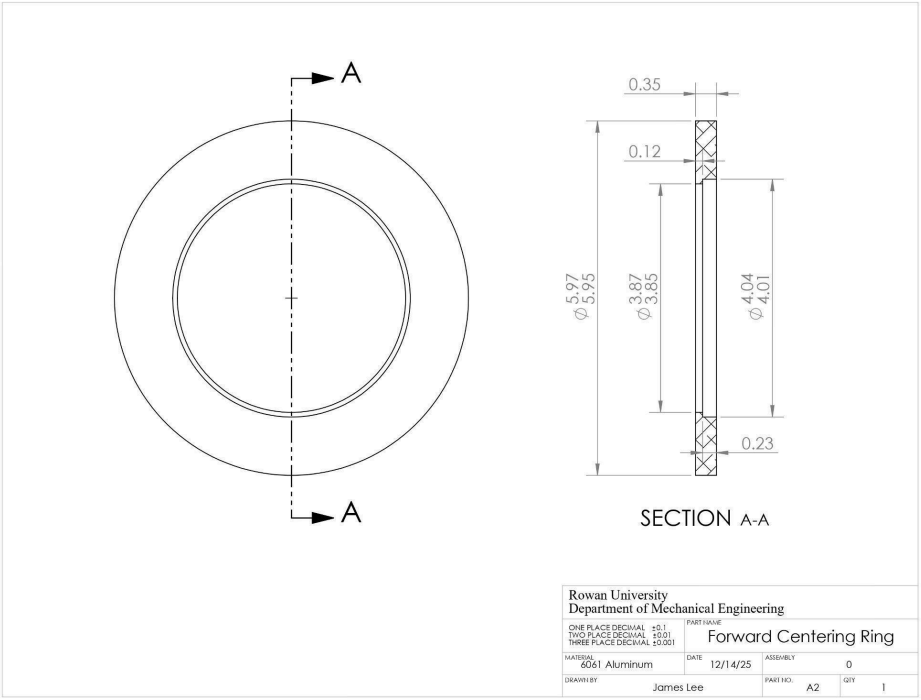


Figure F-K. Forward Centering Ring Drawing

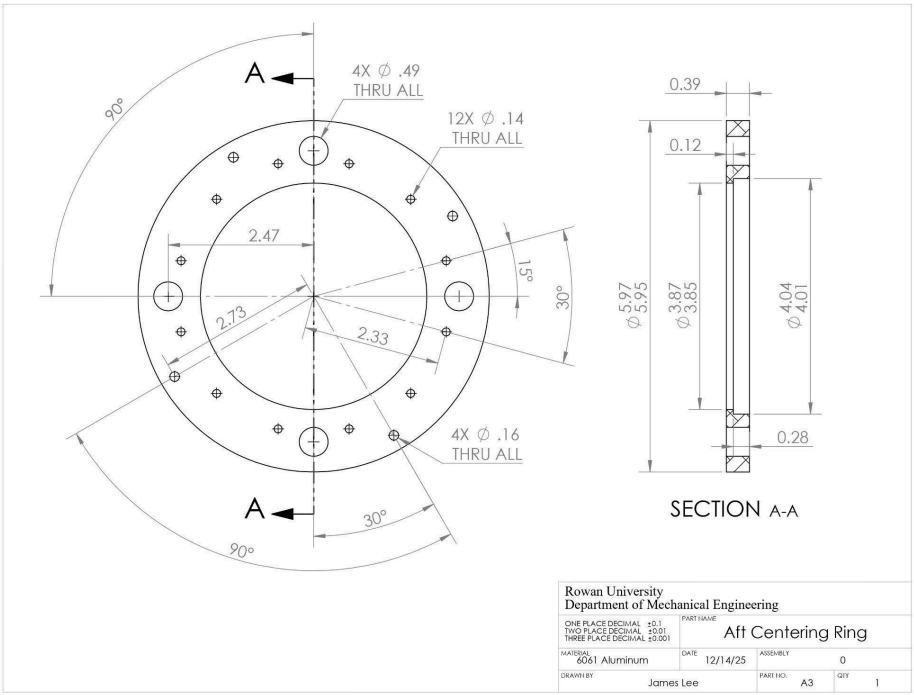


Figure F-L. Aft Centering Ring Drawing

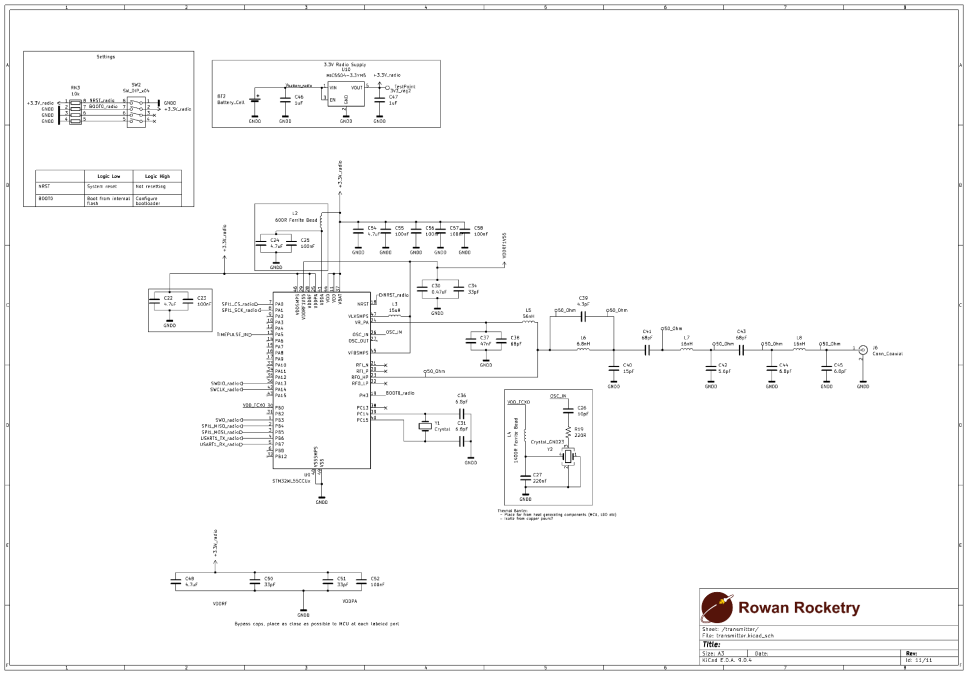


Figure F-M. Transmitter Schematic

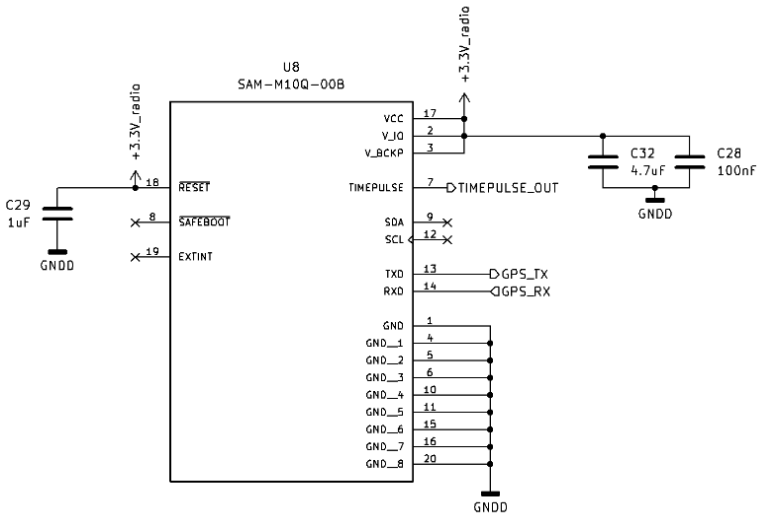


Figure F-N. Implementation of SAM-M10Q Receiver

Rowan Rocketry Avionics/Ground Station
Electronics Diagram

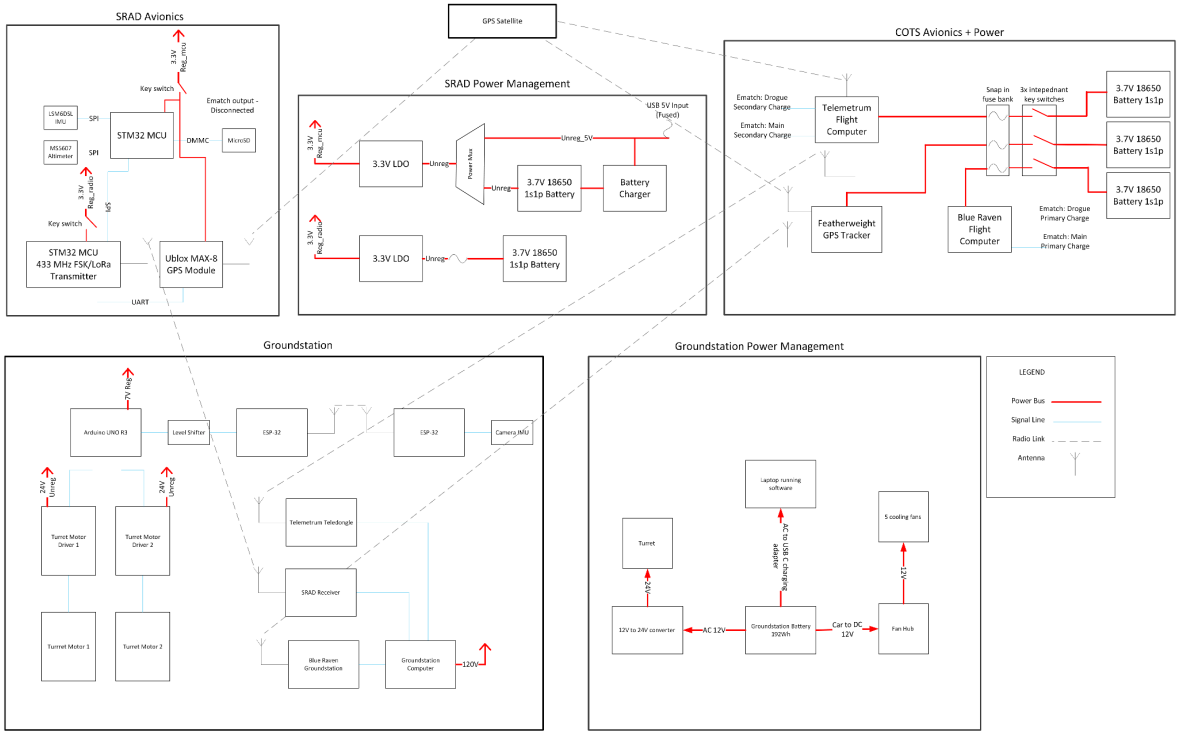


Figure F-O. Full Avionics/Ground Station System Diagram

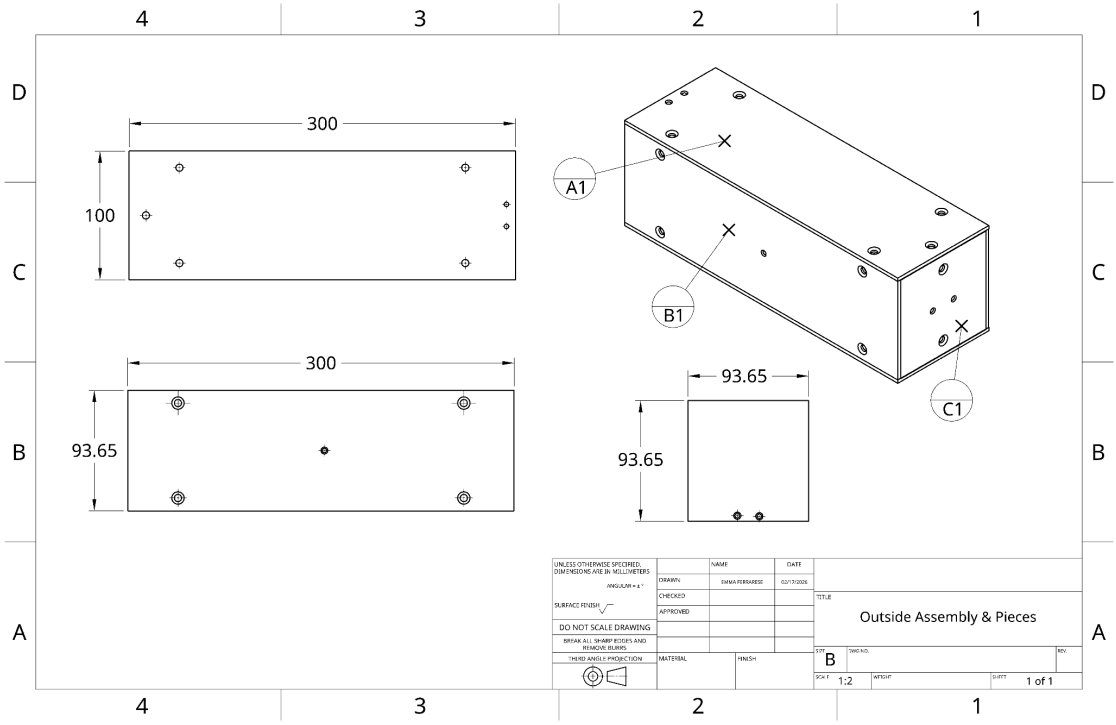


Figure F-P. Payload Assembly Engineering Drawing

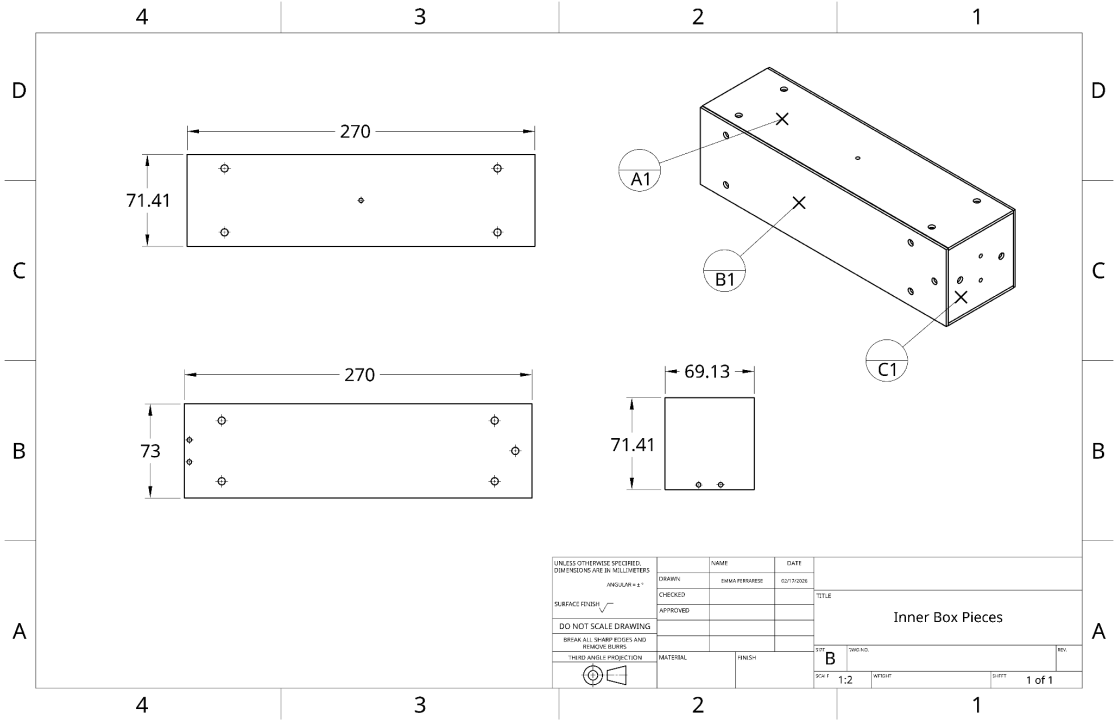


Figure F-Q. Payload Assembly Engineering Drawing

XI. Appendix G

Other

The key for the QFD Decision Matrices in this section and subsequent sections is as follows:

A. Star = Optimal (value of 9)
B. Square = Serviceable (value of 3)
C. Sphere = Substandard (value of 1)

Table G-A. QFD Decision Matrix for Body Tubing Material

Body Material				
Decision Making Criteria	*Blue Tube + Fiberglass Sheet*	*Fiberglass*	*Carbon Fiber*	*Weight*
Durability	🔵	⭐	⭐	20.00%
Cost	⭐	🟥	🔵	15.00%
Weight	🔵	🟥	⭐	20.00%
Dimensional Stability	🔵	⭐	⭐	10.00%
Complexity	🔵	⭐	🔵	10.00%
Machinability	⭐	🟥	🔵	10.00%
RF Compatible	⭐	⭐	🔵	15.00%
TOTALS:	4.2	**6.3**	5	

Table G-B. QFD Decision Matrix for Epoxy Candidates

Epoxy Brand / Type						
Decision Making Criteria	*Aeropoxy ES6209*	*Aeropoxy ES6279*	*Proline 4500*	*US Composites 635*	*Cotronics 4525*	*Weight*
Pot life	⭐	🟥	🔵	🟥	🟥	20.00%
Cure to Working Strength	🟥	⭐	🟥	🔵	🟥	5.00%
Viscosity	🟥	⭐	⭐	⭐	⭐	10.00%
Yield Strength (T)	🟥	🔵	⭐	⭐	⭐	25.00%
Yield Strength (C)	🟥	⭐	⭐	⭐	🔵	25.00%
Cost	🔵	🔵	🟥	⭐	🔵	15.00%
TOTALS:	3.9	4.6	6.2	**7.4**	4.3	

Table G-D. QFD Decision Matrix for Fin Material

Fin Material				
Decision Making Criteria	*G7*	*G10 non FR4*	*G11*	*Weight*
Cost	⭐	⭐	⭐	10.00%
Tensile Strength	🔵	🟥	⭐	15.00%
Compressive Strength	🔵	🟥	🟥	15.00%
Flexural Strength	🔵	🟥	⭐	30.00%
Impact Resistance	⭐	🔵	🟥	30.00%
TOTALS:	4.2	3	**6.3**	

Table G-E. QFD Decision Matrix for Nose Cone Shape

Nose Cone Shape					
Decision Making Criteria	*5:1 Von Karman*	*4:1 Ogive*	*Parabolic*	*3/4 Power*	*Weight*
Drag	🟥	🟥	⭐	⭐	35.00%
Weight	🟥	⭐	🔵	🔵	25.00%
Material	⭐	⭐	🔵	🔵	30.00%
Cost/Availability	⭐	⭐	🔵	🔵	10.00%
TOTALS:	5.4	**6.9**	3.8	3.8	

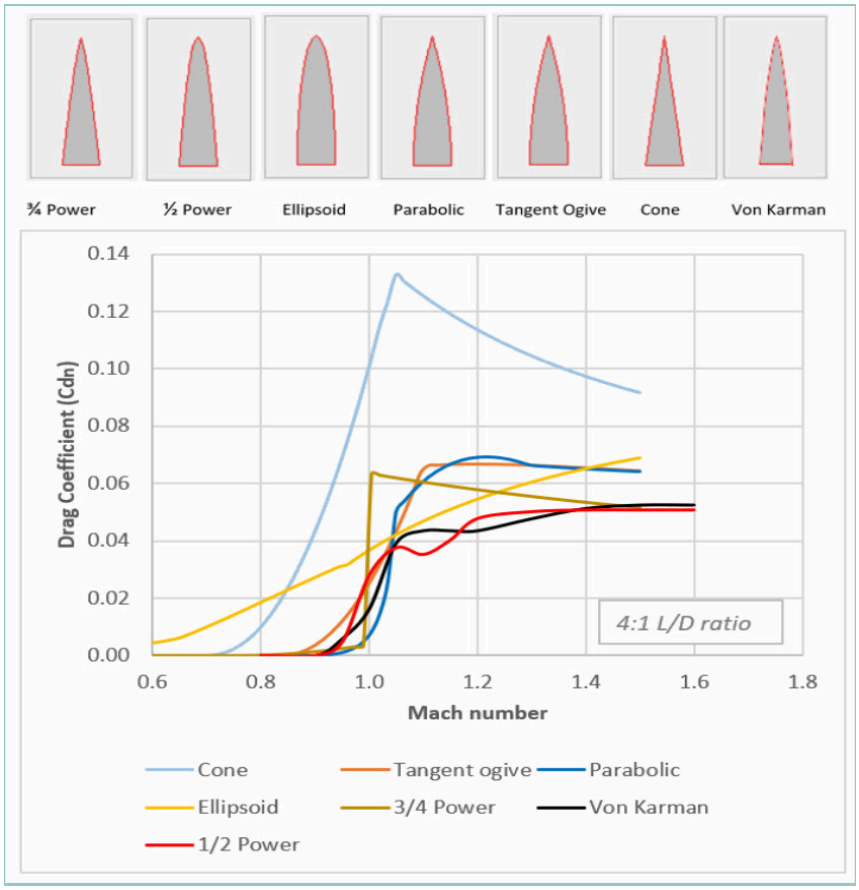


Figure G-F. Nose Cone Profile Drag Coefficient Plot

Table G-G. Material Test Information

Property (Units)	Compression Values Test 1/Test 2 (ASTM D695)	Tension Values Test 1/Test 2 (ASTM D309)	Shear Values Test 1/Test 2 (ASTM D5379)
Yield Stress (MPa)	344/276	210/168	65/60
Modulus (GPa)	19.0/17.0	18.0/15.5	4.0/3.2
Ultimate Strength (MPa)	430/345	310/250	110/85
Failure Strain	2.50/2.00	1.80/1.40	3.20/2.60
Poisson's Ratio	0.13/0.11	0.13/0.11	—

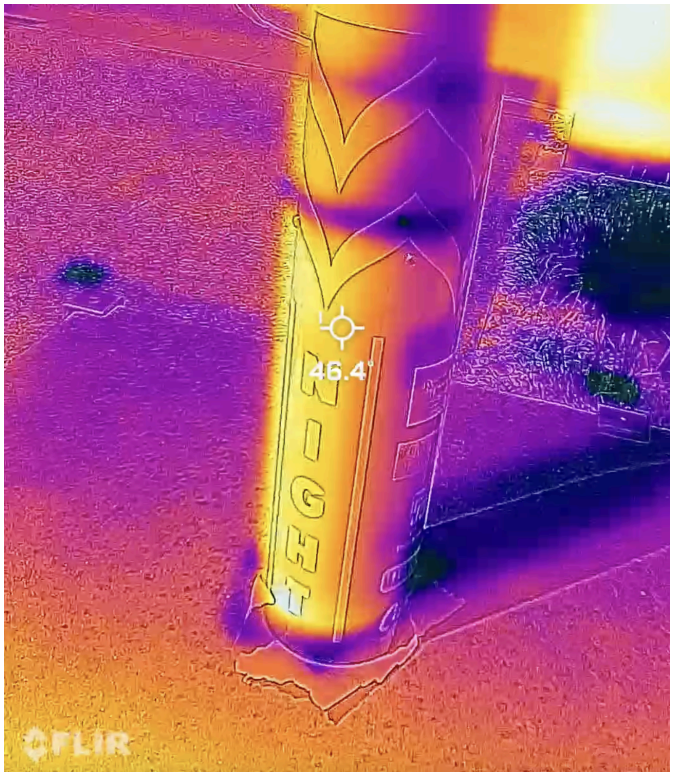


Figure G-H. Thermal Image of the Outside Surface of the Rocket at 31.1°C Ambient Temperature

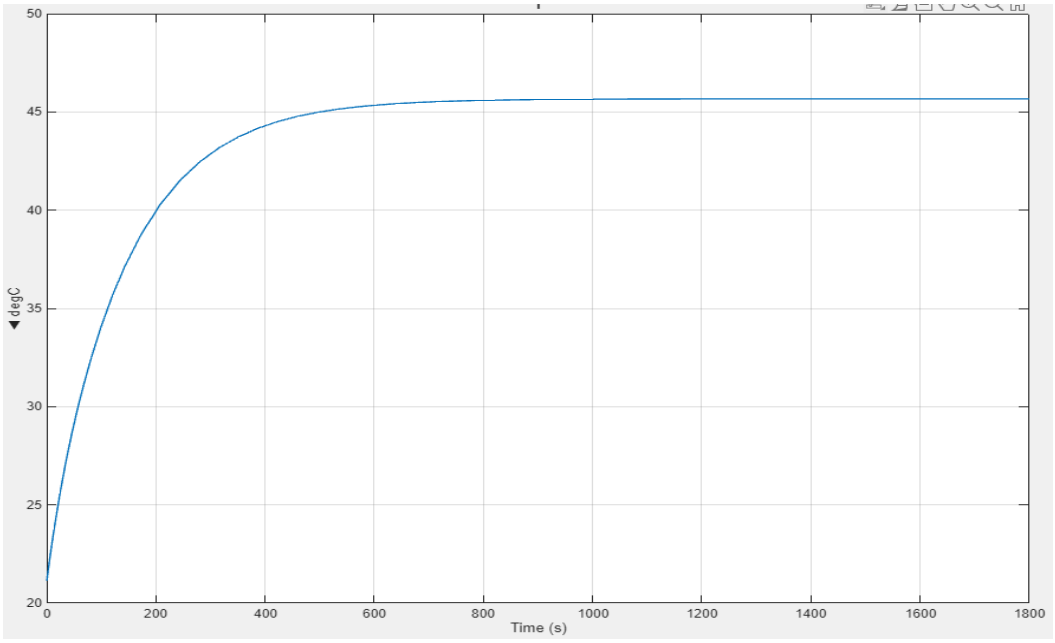


Figure G-I. MATLAB Simulink Prediction of Surface Temperature of the Vehicle at Ambient Temperature of 31.1°C over time

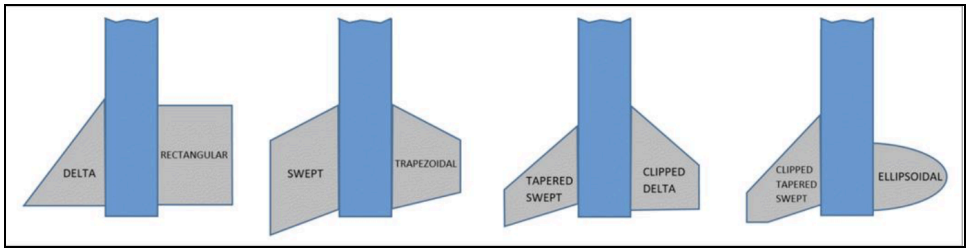


Figure G-J. Types of fin shapes considered for the final design [1]

Type	Pros	Cons
Delta	-Flutter resistant	-Susceptible to damage, -Generates the least force of all the designs
Rectangular	-Flutter resistant, -Easy to make and robust	-Easily damagable
Swept	-Flutter resistant -Robust design	-Susceptible to damage upon landing
Trapezoidal	-Flutter resistant -Robust design -Can shift Cp when clipped	-Less aerodynamic than swept
Tapered Swept	-Ideal for high speeds	-Susceptible to flutter and landing damage
Clipped Delta	-Robust and proven design	-Potentially susceptible to damage upon landing
Clipped Taper Swept	-Improved tapered swept	-Susceptible to flutter and damage upon landing
Ellipsoidal	-Aerodynamically efficient	-Difficult to fabricate and calculate Cp

Figure G-K. Pros/cons comparison of most popular fin shapes used in rocketry [1]

Table G-L. QFD Decision Matrix for Fin Shape

Fin Shape					
Decision Making Criteria	*Trapezoidal #5*	*Trapezoidal #2*	*Tapered #3*	*Tapered #6*	*Weight*
Aerodynamic Efficiency	🟥	🟥	⭐	⭐	20.00%
Durability	⭐	⭐	🟥	🟥	30.00%
Flutter Resistance	🟥	🟥	🔵	🔵	20.00%
Apogee	🟥	🟥	🟥	⭐	10%
Max. velocity	🟥	🔵	⭐	🟥	10.00%
Complexity	🟥	🟥	🔵	🔵	10.00%
TOTALS:	**4.8**	4.6	4.2	4.2	

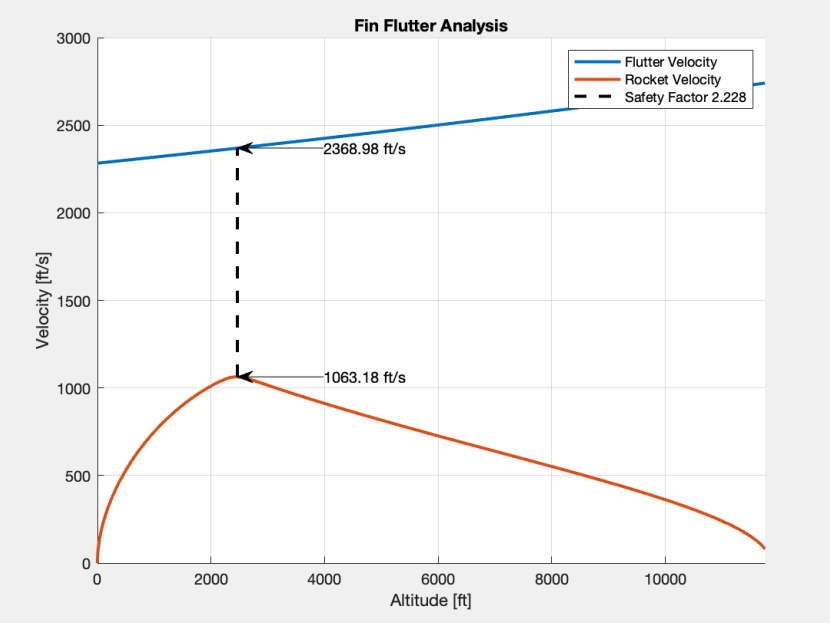


Figure G-M. Current FoS for trapezoidal fins made out of G10 and with 3 layers of CF

Table G-N. Motor Selection Table (Weight [lbs] vs. Apogee [feet])

Weight (lbs)	55	60	65	70	75
M2000R-PS	12,275	11,571	10,653	9,722	8,842
M2500T-PS	12,557	12,053	11,214	10,310	9,427
M1939W-PS	13,917	13,439	12,532	11,542	10,558
M750W-PS	12,530	11,230	9,984	8,829	7,781
M1800FJ-PS	10,914	9,997	9,072	8,200	7,389

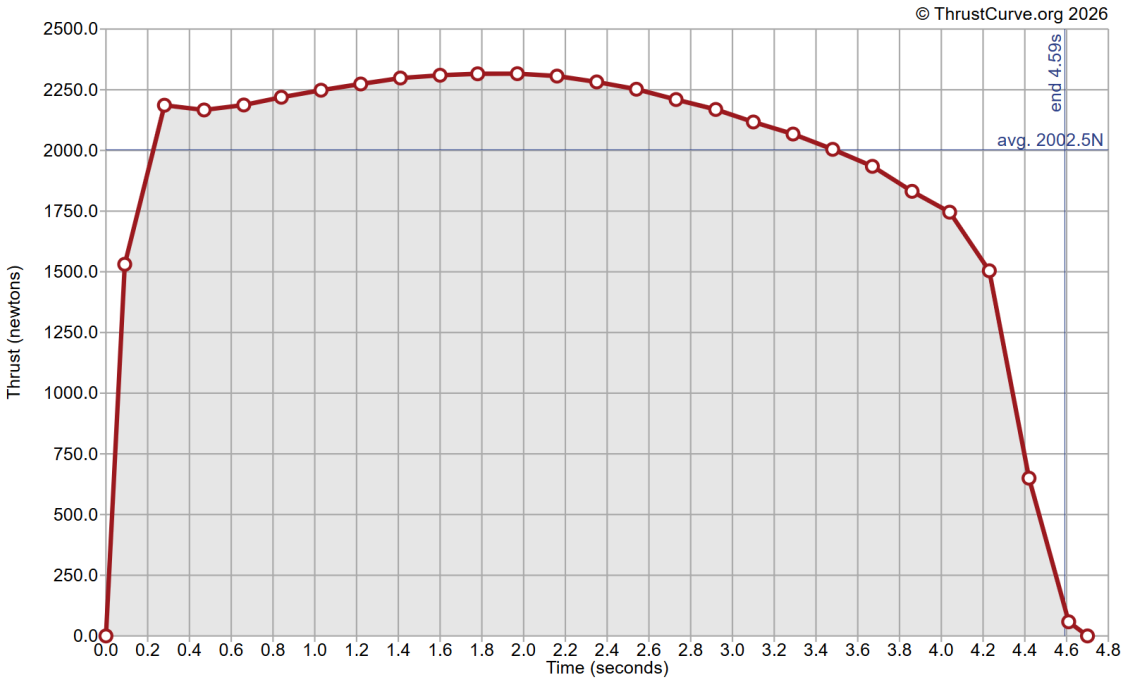


Figure G-O. M2000R Thrust Curve



Figure G-P. Decision Making Matrix for Flight Computers

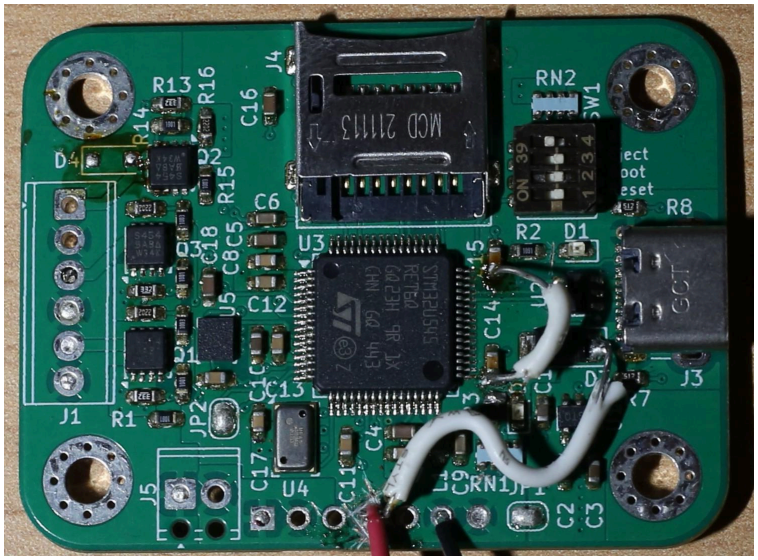


Figure G-Q. Old SRAD flight computer

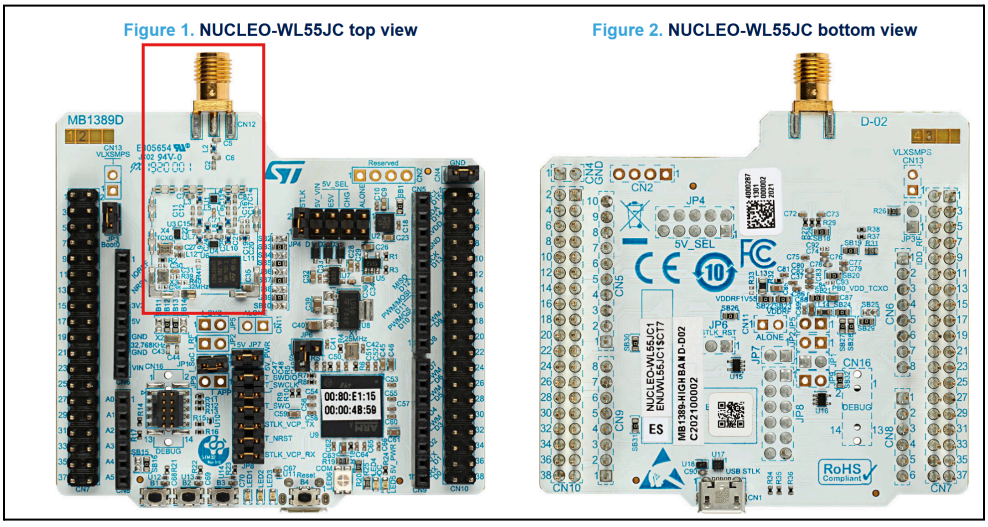


Figure G-R. NUCLEO-WL55JC Reference Design for SRAD Radio transmitter

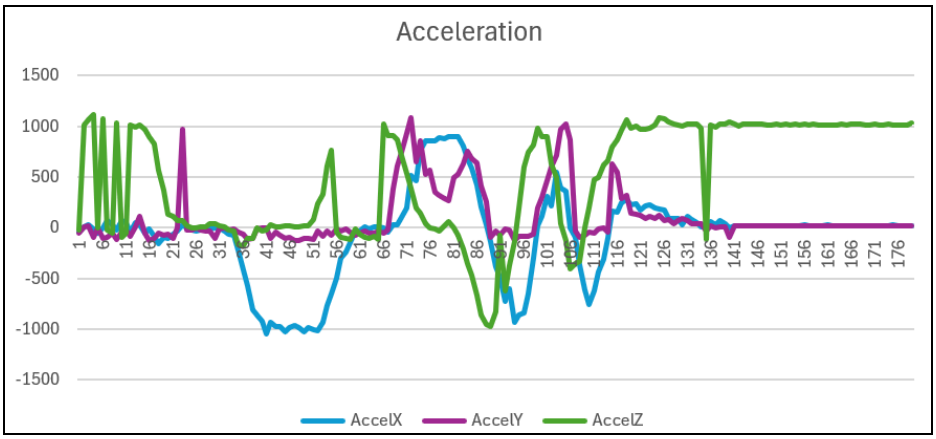


Figure G-S. SRAD raw accelerometer data

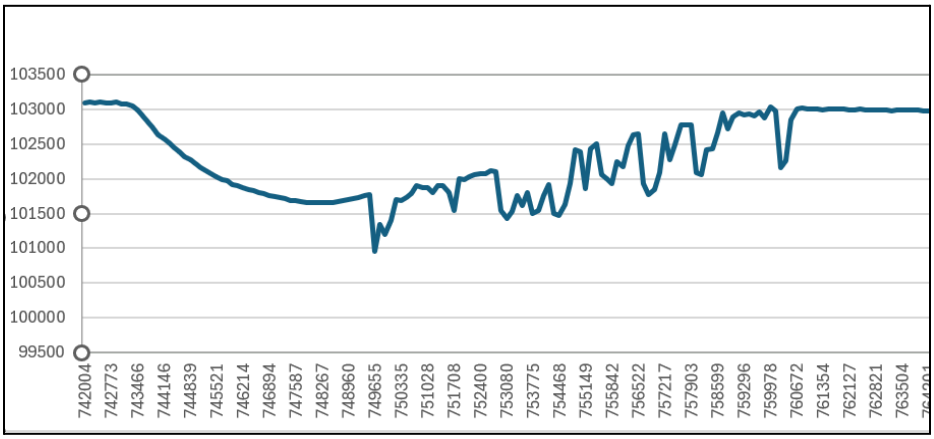


Figure G-T. SRAD raw pressure sensor data



Figure G-U. SRAD GPS path mapping in OpenCPN

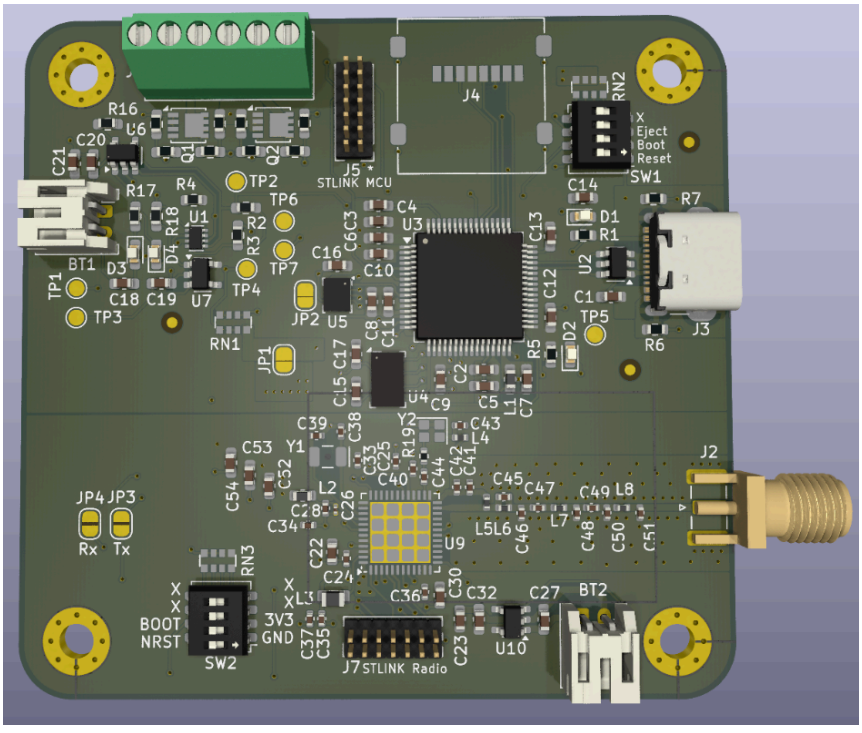


Figure G-V. SRAD Flight computer final form factor board

Table G-W. Possible Parachute Configurations

Main Chute Name	Main Chute Model	Drogue Chute Name	Drogue Chute Model	Motor Configuration	Velocity at Main Chute Deployment (ft/s)	Flight Time (s)	Velocity at Ground Hit (ft/s)	Velocity at Ground Hit (mph)	Snatch Force (lbf)
14 ft Iris Ultra Compact	IFC-168-S	3.5 ft Elliptical Chute	CFC-042-N	M-2000R	56.4	259	13.3	9.07	1230.723
16 ft Iris Ultra Compact	IFC-192-S	4 ft Elliptical Chute	CFC-048-N	M-2000R	50.0	284	11.7	7.98	1263.357
18 ft Iris Ultra	Custom	4 ft Elliptical Chute	CFC-048-N	M-2000R	49.1	300	11.0	7.50	1,541.892
16 ft Iris Ultra Compact	IFC-192-S	3.5 ft Elliptical Chute	CFC-042-N	M-2000R	56.9	260	12.2	8.32	1636.102
14 ft Iris Ultra Compact	IFC-168-S	3 ft Elliptical Chute	CFC-036-N	M-2000R	65.6	232	14.0	9.55	1664.983
18 ft Iris Ultra	Custom	3.5 ft Elliptical Chute	CFC-042-N	M-2000R	56.1	274	11.3	7.70	2,012.874
16 ft Iris Ultra Compact	IFC-192-S	3 ft Elliptical Chute	CFC-036-N	M-2000R	66.2	235	12.4	8.45	2,214.634
18 ft Iris Ultra	Custom	3 ft Elliptical Chute	CFC-036-N	M-2000R	65.2	249	11.1	7.57	2,718.856
18 ft Iris Ultra	Custom	Custom Chute	Custom	M-2000R	182.0	150	11.2	7.64	24,319.811

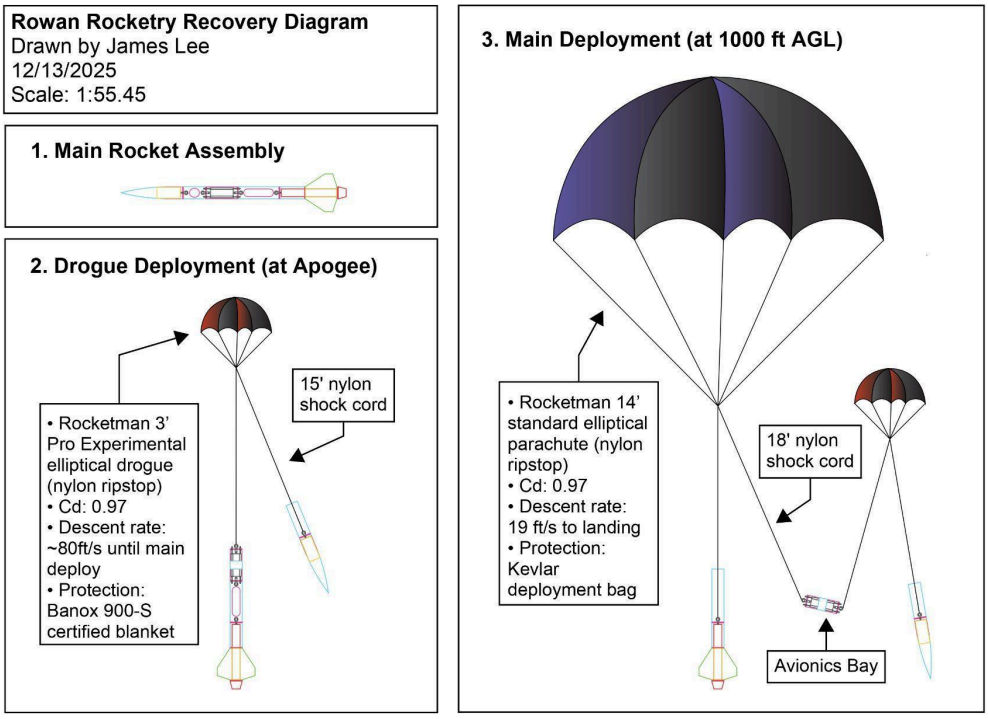


Figure G-X. Recovery Diagram

Atmospheric Density Interpolation

$x_1 = 0\ \text{ft}$

$x_2 = 5000\ \text{ft}$

$$y_1 = 20.48 * 10^{-4}\ \frac{\text{slug}}{\text{ft}^3} = 0.00205\ \frac{\text{slug}}{\text{ft}^3}$$

$$y_2 = 23.77 * 10^{-4}\ \frac{\text{slug}}{\text{ft}^3} = 0.00238\ \frac{\text{slug}}{\text{ft}^3}$$

$x = 2920\ \text{ft} + 1000\ \text{ft} = 3920\ \text{ft}$

$$\rho = y_1 + \frac{(x - x_1) * (y_2 - y_1)}{x_2 - x_1} = 0.00231\ \frac{\text{slug}}{\text{ft}^3}$$

Snatch Force Calculations

$C_d = 0.97$

$d = 168\ \text{in} = 14\ \text{ft}$

$$A = \frac{pi * d^2}{4} = 153.938\ \text{ft}^2$$

$$v = 85.8\ \frac{\text{ft}}{\text{s}}$$

$$F = 0.5 * \rho * C_d * A * v^2 = 1267.388\ \text{lbf}$$

Figure G-Y. Snatch Force Calculations

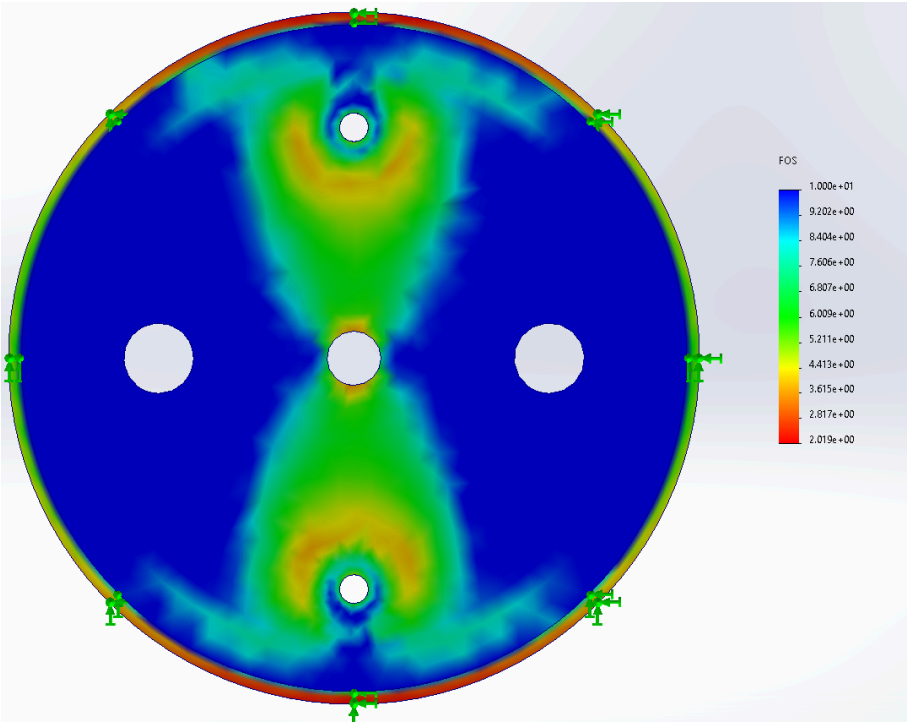


Figure G-Z. FOS Plot for Internal Bulkhead w/ 1250 [lbf] Snatch Force + 840 [lbf] preload

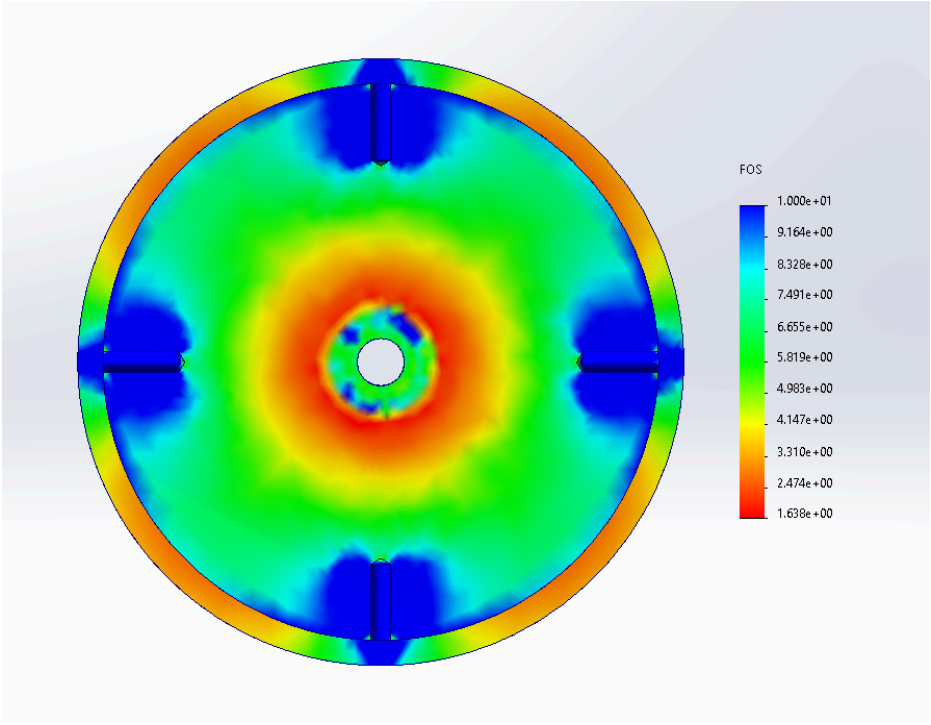


Figure G-AA. FOS Plot for Aft Bulkhead w/ 1250 [lbf] Snatch Force

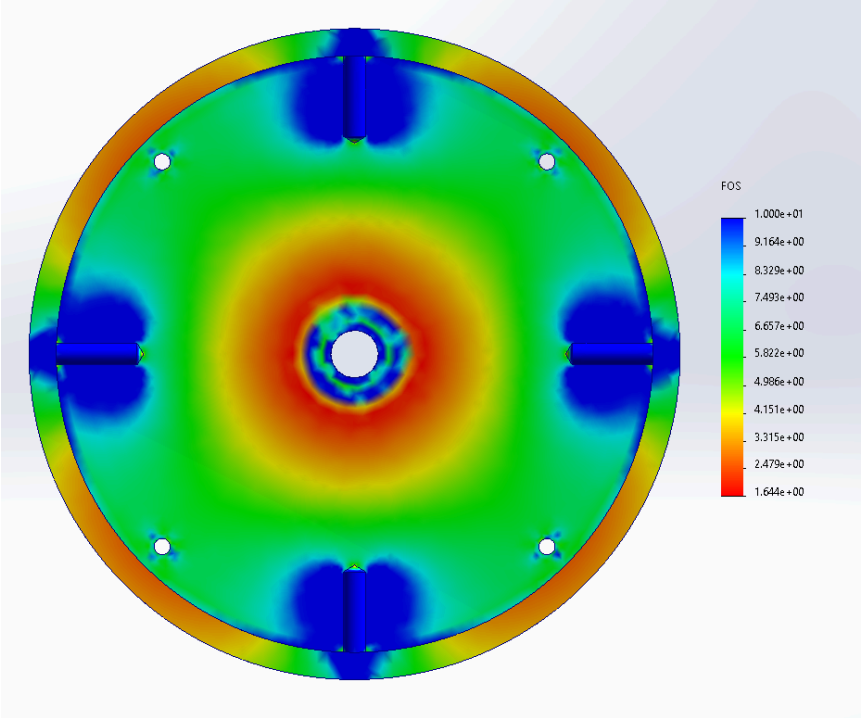


Figure G-AB. FOS Plot for Forward Bulkhead w/ 1250 [lbf] Snatch Force

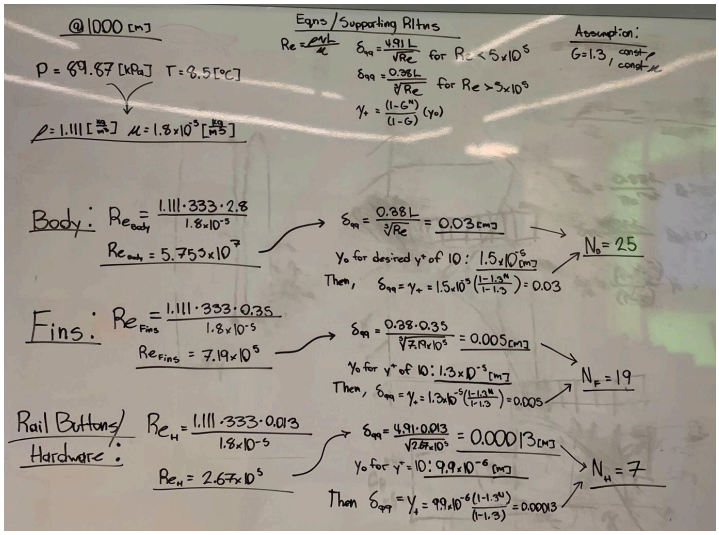


Figure G-AC. Inflation Layer Calcs for Y+ of 10

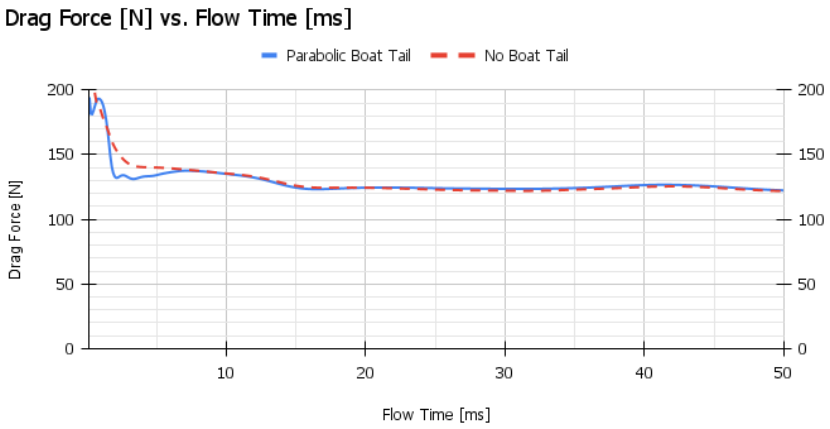


Figure G-AD. Drag Force vs. Flow Time from CFD Simulations

Drag WITHOUT Rail Button Values		
Mean Drag PBT	**RMS Drag PBT**	**Standard Deviation**
126.731	126.807	4.398
Mean Cd PBT	**RMS Cd PBT**	
0.357	0.357	0.012
Mean Drag NBT	**RMS Drag NBT**	
126.732	126.867	5.8545805
Mean Cd NBT	**RMS Cd NBT**	
0.357	0.357	0.0164720423

Standard Error Difference (Drag Force):	***0.337***
Standard Error Difference (Cd):	***0.001***

Mean Difference (Drag Force):	***-0.001***
Mean Difference (Cd):	**0.000**

Figure G-AE. Mean and RMS CFD Drag Values and Error

Acknowledgements

The Rowan Rocketry team would like to thank the faculty and staff of Rowan University for their continued support of the Engineering Clinic program and student-led rocketry efforts. In particular, the team acknowledges the guidance of clinic advisors and faculty mentors, whose technical insight and feedback were instrumental throughout the design and development process.

The team also extends its gratitude to the Rowan University machine shop staff and the Digital Engineering Hub (DEHub) for providing access to advanced manufacturing resources, including machining equipment and metal additive manufacturing capabilities used in the fabrication of critical components such as the charge wells.

Special thanks are given to the Camden County College CIM Center for their collaboration and support in machining fiberglass airframe components, as well as for their contributions to improving fixture design and machining processes. Their assistance was essential in overcoming manufacturing constraints associated with fiberglass materials.

The team would also like to recognize industry partners and suppliers, including Wildman Rocketry and JMJ Profile, for providing materials and technical resources that supported the development of the vehicle.

Finally, the team acknowledges the contributions of past Rowan Rocketry members, whose prior designs, analysis tools, and lessons learned provided a strong foundation for this year's vehicle. Their work continues to shape the team's evolution toward more rigorous and reliable engineering practices.

References

[1] mtnmanak, “Carbon fiber vinyl film wrap instead of Paint | Rocketry Forum - Model Rocketry Forums,” The Rocketry Forum, https://www.rocketryforum.com/threads/carbon-fiber-vinyl-film-wrap-instead-of-paint.166178/ (accessed Apr. 9, 2026).

[2] F.-T. Designs, “Can Car Wrap Withstand the Sun and High Temperatures?,” Fast-Trac Designs , https://fast-tracdesigns.com/car-wrap-withstand-the-arizona-sun-and-high-temperatures/ (accessed Apr. 9, 2026).

[3] S. Public, “Painting Rockets: Star Public,” Star Republic, https://rocketry.gitbook.io/public/tutorials/airframe/painting-rockets (accessed Apr. 9, 2026).

[4] C. P. Cleveland, “Vinyl Wrap vs. Paint: Which One Lasts Longer?,” Ceramic Pro Cleveland, https://www.ceramicprocle.com/vinyl-wrap-vs-paint-which-one-lasts-longer/#:~:text=While%20vinyl%20wraps%20provide%20great,excellent%20protection%20against%20the%20elements. (accessed Apr. 9, 2026).

[5] P. O. Parts, “Paint Care Guide for Black and Dark-Colored Vehicles,” Painted OEM Parts, https://www.paintedoemparts.com/post/paint-care-guide-for-black-and-dark-colored-vehicles?srsltid=AfmBOopJA1cucc_Getgg6W-kOB_OItMTnVonRdR3jOnnAFE6jf5uCLp3 (accessed Apr. 9, 2026).

[6] “Surface Radiation Absorptivity,” The Engineering Toolbox, https://www.engineeringtoolbox.com/radiation-surface-absorptivity-d_1805.html (accessed Apr. 21, 2026).

[7] “Richard Nakka’s experimental rocketry site.” https://www.nakka-rocketry.net/fins.html (accessed Apr. 30, 2026)

[8] “AeroTech M2000R,” *ThrustCurve.org*. [Online]. Available: https://www.thrustcurve.org/motors/AeroTech/M2000R/. (Accessed: Apr. 30, 2026).

[9] “Standard Atmosphere - Pressure and Density,” ATSC 113, https://www.eoas.ubc.ca/courses/atsc113/flying/met_concepts/02-met_concepts/02a-std_atmos-P/index.html. (Accessed: Dec. 29, 2025).

[10] “THE DESCRIPTIVE GEOMETRY OF NOSE CONES,” 1996, Gary A. Crowell Sr. http://servidor.demec.ufpr.br/CFD/bibliografia/aerodinamica/Crowell_1996.pdf. (Accessed: Jan. 15, 2026).